Spatial Transcriptomics Reveals that the Local Immune Response to Placental Guinea Pig Cytomegalovirus Infection is Driven by Chemokine Signaling

Zachary W. Berkebile,[1] Colleen L. Forster,[2] Emma Stanley,[3] Fernanda M. Rodriguez,[3] Adam C. Herman[4], Micah D. Gearhart[5], Craig J. Bierle[1]*

[1.] Division of Pediatric Infectious Diseases, Department of Pediatrics, University of Minnesota, Minneapolis, Minnesota, United States of America

[2.] Biorepository and Laboratory Services, Clinical and Translational Science Institute, University of Minnesota, Minneapolis, Minnesota, United States of America

[3.] University of Minnesota Genomics Center, Department of Pediatrics, University of Minnesota, Minneapolis, Minnesota, United States of America

[4.] Minnesota Supercomputing Institute, University of Minnesota, Minneapolis, Minnesota, United States of America

[5.] Division of Maternal-Fetal Medicine, Department of Obstetrics, Gynecology and Women's Health, University of Minnesota, Minneapolis, Minnesota, United States of America

* Corresponding Author

E-mail: cjbierle@umn.edu

Short title: Spatial Transcriptomics of GPCMV-infected placentas

Abstract

Cytomegalovirus infection can disrupt placental development and function either by directly infecting placental cells or by eliciting a pathogenic immune response. The relative contributions of these two mechanisms to adverse pregnancy outcomes remains poorly understood. In this study, we used spatial transcriptomics to quantify host and viral gene expression at the maternal-fetal interface at near single-cell resolution. Guinea pig cytomegalovirus (GPCMV) infection after mid-gestation causes focal infections at the base of the main placenta. Samples for spatial transcriptomics were collected from guinea pigs infected with GPCMV at 35 days gestation. Viral loads and the location of infected cells in placentas were assessed using virus-specific droplet digital PCR and *in situ* hybridization at 21 days post-infection. Representative placentas were sectioned onto Visium Spatial Gene Expression Slides and sequencing libraries were prepared from six infected and six uninfected tissue sections. Spatial transcriptomes from 33,687 55-μm spots were generated and used in subsequent analyses. To assess how infection affected gene expression at the maternal-fetal interface, a combination of graph-based clustering and manual classification was used to assign spatial transcriptomes to clusters representative of different anatomic regions. Infection dysregulated more transcripts in the decidua and junctional zone than in the labyrinth or non-capillarized syncytium. Notably, infection downregulated transcripts involved in lipid metabolism and upregulated transcripts involved in antiviral defense and chemokine signaling. A second analysis compared the spatial transcriptomes of GPCMV-infected cells and their immediate microenvironment with similar regions in uninfected placentas. A transcriptional signature indicative of immune activation was clear in this comparison, and the local placental response to cytomegalovirus infection was driven by upregulated chemokine signaling. Thus, spatial transcriptomics revealed regional patterns of gene expression in the guinea pig placenta and illuminated how the host response to GPCMV may compromise placental function.

Author Summary

The placenta supports fetal development while also acting as an immune barrier against bloodborne pathogens. Cytomegalovirus (CMV), the most common viral cause of congenital infections and preventable neurologic disability in children, evades host defenses to infect the placenta. How CMV affects the placenta and fetal health remains poorly understood. Using a guinea pig model of CMV infection during pregnancy and spatial transcriptomics, a recently-developed method that enables gene expression to be studied at near-cellular resolution, this study compared normal and infected placentas. The effects of infection on directly infected cells and their immediate environment and indirect effects that occur at more distant sites were revealed. This information may inform the development of therapies to improve placental function after CMV infection.

Introduction

Human cytomegalovirus (HCMV) is a ubiquitous herpesvirus and the most frequent cause of congenital viral infections [1]. Congenital cytomegalovirus (cCMV) infections occur in roughly 1 in 200 pregnancies and approximately 8000 children are disabled by cCMV each year in the United States [2]. Placental infection plays a central role in the pathogenesis of cCMV. The placenta is critical for supporting fetal development, facilitates the development and maintenance of maternal tolerance, and acts as an immunologic barrier protecting the developing offspring from bloodborne pathogens. A myriad of antiviral defenses, including the constitutive expression of pattern recognition receptors and type III interferon, prevent most viruses from replicating in the placenta and/or infecting the fetus [3]. HCMV can infect both the maternal decidua and the placenta, placental infection likely precedes congenital infection, and

68 some adverse pregnancy outcomes, including fetal growth restriction and stillbirth, can be
69 caused by placental HCMV infections that do not transmit to the fetus [4-7].

70 How HCMV infection affects placental development and function remains poorly
71 understood [8]. In clinical samples, HCMV antigens are most often detected in the decidua, in
72 cytotrophoblasts located in floating villi and cell columns, and in the villous stroma and fetal
73 capillaries [9, 10]. Villous malformations have been noted in cases of early fetal demise after
74 congenital HCMV infection, and it has been proposed that infection can interfere with
75 trophoblast proliferation and differentiation to compromise the early placental development [4].
76 Other less severe pathologies, including a hypoxia-like syndrome, are more frequent and
77 observed when placental infection occurs later in pregnancy [5, 11]. Isolated primary extravillous
78 trophoblasts, cytotrophoblasts, and trophoblast progenitor cells can be productively infected by
79 HCMV *in vitro* [12-15]. Infection reduces the capacity of cytotrophoblasts to proliferate, limits the
80 differentiation of trophoblast progenitor cells, and interferes with the anchoring of villous
81 explants *in vitro* [16, 17]. HCMV can infect trophoblast stem cells, where the virus dysregulates
82 the expression of transcripts involved in differentiation, but these infections are not productive,
83 have no apparent effect on the proliferation of the trophoblast stem cells, and viral genomes are
84 not maintained after passage [18, 19]. Similar observations have been made in trophoblast
85 organoids, which also do not support productive HCMV replication [20].

86 The inflammatory response to placental infection can cause pregnancy loss, growth
87 restriction, neurocognitive impairment, and developmental delay [21]. Proinflammatory cytokines
88 accumulate in amniotic fluid, the placenta, and maternal sera during congenital HCMV infections
89 [22-24]. Similar inflammatory responses occur when tissue explants and organoids are infected
90 with HCMV *in vitro* [20, 25, 26]. Therapeutic or genetic interference with inflammatory signaling
91 pathways can rescue murine pregnancies after infection, exposure to pathogen associated
92 molecular patterns, or cytokines treatments [27, 28]. The species-specificity of HCMV and

93 inability of mouse cytomegalovirus to cause placental and congenital infections has limited our
94 ability to experimentally study whether the inflammatory response to placental infection is a
95 cause of fetal harm [1, 29].

96 Guinea pigs are the most widely used animal model of cCMV infection. Guinea pigs
97 have ~65-day gestational periods and highly-developed, precocious offspring [30]. Major guinea
98 pig organ and immune systems develop *in utero* to an extent that is more like humans than the
99 mouse or rat. Guinea pig cytomegalovirus (GPCMV, also known as Caviid herpesvirus 2) was
100 isolated from the salivary gland of an infected guinea pig and primary GPCMV infection during
101 pregnancy leads to the sequential infection of the placenta and fetus [31-35]. Fetal outcomes
102 are affected by the timing of infection during pregnancy [36, 37]. Notably, maternal infection
103 after mid-gestation causes high rates of stillbirth and fetal growth restriction, and lesions,
104 including ischemic injury and areas of necrosis, are observed in GPCMV-infected placenta at 14
105 days post-infection (dpi) and later [33]. We recently compared how maternal GPCMV infection
106 either late in the embryonic period (21 days gestation [dGA]) or after mid-gestation (35 dGA)
107 affected the placenta [38]. While there were no significant differences in viral genome
108 abundance between these two groups at 21 dpi, bulk RNA-seq revealed that significant
109 changes in placental gene expression were largely restricted to the animals that had been
110 infected at 35 dGA. *In situ* hybridization further revealed differences in the location of infected
111 cells in older and younger placenta. These observations led us to hypothesize that the guinea
112 pig placenta becomes sensitized to infection late in gestation, when a population of GPCMV-
113 susceptible cells develop near the base of the main placenta, and that the immune response to
114 these infected cells compromises placental function.

115 In this study, we used spatial transcriptomics to compare gene expression in age-
116 matched GPCMV-infected and control placentas at a near-cellular resolution. We found that
117 infection affects gene expression in anatomic regions, such as the labyrinth, that are not directly

118 infected by the virus. When gene expression was compared between GPCMV-infected cells and
119 their immediate microenvironment and a comparable area in mock-infected placentas, we found
120 that the local inflammatory response to GPCMV was driven by upregulated chemokine gene
121 expression. Similarities in the placental response to CMV infection between humans and guinea
122 pigs indicate that the rodent could be a valuable model for testing immunomodulatory therapies
123 that aim to prevent fetal injury after chronic placental infections.

124 Results

125 Spatial transcriptomics of the guinea pig placenta

126 HCMV and GPCMV both cause focal infections in the placenta [10, 33, 38]. When virus-
127 specific immunohistochemistry or *in situ* hybridization is used to detect GPCMV, individual
128 infected cells or small groups of infected cells can be detected in both the placenta and decidua
129 but are rare [33, 38-40]. However, we have found that comparably large areas of infected cells
130 can be consistently detected at the base of the main placenta when dams are infected after mid-
131 gestation and euthanized near term [38]. These cells are often found adjacent to the
132 subplacenta or maternal arterial channels that perfuse the placenta. We utilized the Visium
133 Spatial Gene Expression platform (10x Genomics) to study transcription in the guinea pig
134 placenta and decidua at a near single-cell resolution and illuminate how infection directly and
135 indirectly affects gene expression. This next generation sequencing-based technology uses
136 glass slides tiled with 55 μm diameter, oligonucleotide-containing spots; each capture area
137 contains 5000 of these spots in a 6.5 x 6.5 mm^2 square. The oligonucleotides include location-
138 based barcodes, unique molecular identifiers, and poly-T sequences that are used to capture
139 spatial transcriptomes [41]. **Figure 1** summarizes the experimental approach used in this
140 project. Placentas were collected from guinea pigs that were bred during postpartum estrus,
141 either GPCMV- or mock-infected at 35 days gestation (dGA), and euthanized 21 days post-

142 infection (56 dGA) [42]. One half of each placenta was flash frozen in OCT compound for
143 histopathologic studies and spatial transcriptomics (ST). A portion of the remaining placenta
144 was collected for DNA extraction; extracted DNA was used for viral load quantification and fetal
145 sex screening by droplet digital PCR (ddPCR) and endpoint PCR [43, 44]. For ST, the flash
146 frozen tissue was sectioned onto Visium slides, hematoxylin and eosin (H&E) stained, and
147 imaged. The tissue was then permeabilized and an Illumina sequencing library was generated
148 from cDNA synthesized using the oligonucleotides that are tiled on the capture area.

149 **Figure 1. Spatial transcriptomics workflow.** Gestational age-matched placentas from
150 GPCMV- and mock-infected guinea pigs were divided and flash frozen in OCT
151 compound. Visium Tissue Optimization Slides were used to determine the ideal
152 incubation time for tissue permeabilization and on-slide cDNA synthesis. GPCMV-
153 specific RNAscope was used to screen placentas for GPCMV-infected cells and select
154 representative tissue to analyze on Visium Gene Expression Slides. Placentas were
155 sectioned onto these slides, H&E stained, and imaged. After on-slide cDNA synthesis
156 and Illumina sequencing, data was analyzed using Space Ranger and Partek Flow
157 software. Gene expression in GPCMV- and mock-infected tissue was compared after
158 graph based clustering and spatial transcriptomes that contained infected cells were
159 identified based on their viral read content.

160 On-slide cDNA synthesis was optimized using Visium Tissue Optimization Slides (10x
161 Genomics). Fluorescence microscopy revealed that more cDNA was produced from the main
162 placenta than either the decidua or the subplacenta**,** regardless of how long the tissue had been
163 incubated with permeabilization buffer (**Fig. 1**). This reflects the higher RNA content of the
164 placenta, and we have observed that an average of 2.5±0.71-fold more RNA is extracted per
165 mg of placenta than decidua in other unpublished experiments.

166 RNAscope specific to the viral transcript *gp3* was used to screen for infected cells and
167 identify representative GPCMV-infected samples (**S1 Fig.**); five placentas (three female and two
168 male) collected from three dams were selected for ST. GPCMV-infected cells were detected at
169 the base of the main placenta in all these placentas. Six age-matched placentas from three
170 mock-infected dams were used as controls. The guinea pig placenta is significantly larger than
171 6.5x6.5 mm^2 at 56 dGA and each placenta was trimmed to so that portions of the placenta,
172 decidua, and subplacenta would be included on each capture area. However, examination of
173 the H&E-stained gene expression slides revealed that the subplacenta was not present in
174 several tissue sections (**S2 Fig.**). To verify that infected cells were present in each capture area,
175 a serial section was collected from each trimmed placenta and used for a second round of
176 RNAscope (**S3 Fig.**). In the initial RNAscope analysis, one placenta (2395B) had a large area of
177 *gp3*$^+$ cells in the decidua; this placenta was divided and sectioned onto two capture areas.
178 Sample 2395B1, which should have corresponded to this area of infected decidua, did not
179 contain gp3$^+$ cells in the second round of RNAscope. GPCMV infected cells were detected
180 where expected in all other samples.

181 cDNA from the twelve capture areas was used to prepare sequencing libraries, pooled,
182 and sequenced. Apart from sample 735B, more than $5X10^4$ reads were sequenced per spot and
183 a median of 3900 host transcripts were detected in each spatial transcriptome (**S1 Table**). In
184 GPCMV-infected placentas, a median of $1.45X10^5$ (range $3X10^3$ to $2.6X10^5$) reads mapped to
185 the viral genome per sample. These reads mapped to the 3' end of viral transcripts and
186 spanned the entire GPCMV genome (**Fig. 2**). Fewer than 100 reads mapped to the viral
187 genome in mock-infected tissue sections and these reads were generally highly repetitive
188 sequences.

189 **Figure 2. GPCMV sequences detected in spatial transcriptomes aligned to the viral**
190 **genome.** Sequencing reads were aligned to the GPCMV genome (NC_020231.1) using

SpaceRanger and visualized with Geneious (v11.1.5). The total number of reads mapping to the viral genome in each sample is shown. Coverage at each nucleotide position is graphed in log scale. Regions with coverage <1 read are highlighted in blue and >100 in orange.

GPCMV infection alters gene expression across the distinct anatomic regions of the guinea pig maternal-fetal interface

A combination of graph-based clustering and manual refinement was used to compare gene expression across the different anatomic regions of the guinea pig placenta. The 3000 most variant guinea pig transcripts were used for graph-based clustering; viral transcripts were excluded from this analysis. Ten clusters were produced when a resolution setting of 0.5 was used for graph-based clustering (**S4 Fig.**). Cluster assignment generally reflected where spatial transcriptomes originated at the maternal-fetal interface. The computationally generated clusters were then manually refined. Firstly, data from spatial transcriptomes located in folded tissue or near large blood spaces were excluded from later analyses. Three clusters that included the interlobar or marginal syncytium were combined into a single cluster representative of all non-capillarized syncytium and three clusters were combined and classified as parts of the placental stem and junctional zone. Seven clusters remained after manual spot reassignment (**Fig. 3**). While this underrepresents the complexity of the placenta, a conservative approach allowed us to compare gene expression across many spatial transcriptomes per cluster. The capillarized syncytium was represented by two clusters that comprise the core and periphery of the labyrinth. The non-capillarized syncytium and subplacenta were each represented by a single cluster. The remaining transcriptomes, located in the junctional zone, the stem of the placenta, and the decidua, formed three clusters, the smallest of which was comprised of only 389 transcriptomes and was excluded from later analyses. Consistent with our observation that the

215 subplacenta was not sampled in several tissue sections, spots assigned to the subplacenta
216 cluster were not present in all twelve capture areas (**Fig. 4a**).

217 **Figure 3. Gene expression in spatial transcriptomes reflects their location at the**
218 **maternal-fetal interface.** Spatial transcriptomes were classified using a combination of
219 graph-based clustering and manual reassignment. (**A**) UMAP projection showing
220 transcriptomes colored by the cluster assignment used for differential expression
221 analyses. LP- labyrinth periphery, LC- labyrinth core, NS- non-capillarized syncytium,
222 DE- decidua, SP- subplacenta, N/A- not assigned, JZ-junctional zone and placental
223 stem. **(B)** UMAP projection showing spots colored by sample identifier, with GPCMV-
224 infected samples labeled in red, illustrating the integration of data from three Visium
225 slides and twelve capture areas. **(C)** Representative sections of mock- and GPCMV-
226 infected placenta. The H&E stained tissue sections are shown on the left. Spatial
227 transcriptomes were colored by cluster assignment in the panels on the right.
228 Transcriptomes that were excluded from subsequent analyses are not colored.

229 **Figure 4**. **GPCMV infection dysregulates gene expression in the placenta and**
230 **decidua.** Gene expression was compared between sections of GPCMV- and mock-
231 infected placenta (N=6/group). **(A)** The proportion of spatial transcriptomes in each
232 capture area that were assigned to a given cluster is illustrated by bar chart. **(B)**
233 Transcripts that were differentially regulated by GPCMV infection in each cluster were
234 identified by gene-specific analysis (two-fold or greater change, $p \leq 0.05$). The total
235 number of spatial transcriptomes from GPCMV- and mock-infected capture areas
236 included in this analysis and number of genes that were up- or down-regulated in each
237 comparison are shown.

238 Cluster-specific biomarkers were identified by using Student's t-tests to compare gene
239 expression in the spatial transcriptomes assigned to one cluster with the combined data from all

240 other spatial transcriptomes. **S2 Table** ranks the top 20 biomarkers for each cluster by
241 significance and fold change. To illustrate how biomarker expression varies in the placenta and
242 decidua, expression data for select biomarkers was overlaid onto images of representative
243 control and GPCMV-infected placentas (**S5 Fig.**). The biomarkers for the two labyrinth clusters
244 were partially overlapping. Conversely, the decidua and subplacenta clusters both had a high
245 number of highly expressed biomarkers that were unique to the regions. Interestingly, several
246 prolactin-like transcripts were identified as biomarkers for the labyrinth and non-capillarized
247 syncytium. Guinea pigs, like murid rodents and ruminants, have an expanded prolactin locus
248 and two of these transcripts, *Prlrp1* and *Prlrp2,* were previously shown to be expressed in the
249 guinea pig placenta [45]. Our analysis found that *Prlrp1* was a biomarker for the labyrinth
250 clusters and *Prlrp2* was enriched in the non-capillarized syncytium but expressed at a high level
251 throughout the placenta and decidua. A third, previously uncharacterized prolactin-like
252 transcript, *Ghc2* (LOC111754958), was a biomarker of the non-capillarized syncytium. These
253 prolactin-like transcripts may have evolved to regulate placental development in guinea pigs.

254 To assess how GPCMV infection affected gene expression in the different regions of the
255 placenta, the spatial transcriptomes of infected and mock-infected tissues were compared on a
256 cluster-by-cluster basis. For this analysis, gene expression data was normalized to counts per
257 million plus one and $\log_2$ transformed. Differentially regulated transcripts were identified by
258 gene-specific analysis. Broadly, GPCMV infection downregulated more host transcripts than it
259 upregulated (**Fig. 4b**). Functional enrichment analyses of the differentially regulated transcripts
260 was done with g:Profiler [46]. Infection had a comparably modest effect on gene expression in
261 the labyrinth, the non-capillarized syncytium, and the subplacenta. Several terms related to an
262 antiviral response, including immune response (GO:0006955), type I interferon production
263 (GO:0032606), and chemokine activity (GO:0008009), were enriched in these three regions
264 after GPCMV infection (**S5 Fig.**). Terms related to metabolic functions such as peptidase

265 activity, sterol transport, and signaling receptor binding and activity also were enriched in these
266 clusters. GPCMV-infected cells were rarely detected in these regions by RNAscope and few of
267 the spatial transcriptomes assigned to these clusters contained viral reads. Thus, it can be
268 inferred that infection-associated changes in gene expression in the labyrinth, non-capillarized
269 syncytium, and subplacenta are largely indirect effects of viral infection elsewhere in the
270 placenta.

271 GPCMV infection affected markedly more transcripts in the two clusters that mapped to
272 the decidua or placental stem and junctional zone. Most GPCMV-infected cells were assigned
273 to the later cluster and 74 immune response (GO:0006955) transcripts, including many involved
274 in chemokine signaling, were dysregulated by infection (**Fig. S5**). Viral infection downregulated
275 transcripts with functions related to protein binding (GO:0005515), lipid transport activity
276 (GO:0005319), small molecule metabolic processes (GO:0044281), and developmental
277 processes (GO:0032502) in these tissue compartments. Taken together, this differential gene
278 expression analyses revealed how GPCMV infection affects regions of the placenta that are not
279 directly infected. While GPCMV infection dysregulates fewer transcripts in the main placenta
280 than in the decidua, placental stem, or junctional zone, the upregulation of *Irf7* and select
281 interferon stimulated genes (e.g. *Isg15*, *OasL*, and *Rsad2*) provides evidence that an antiviral
282 response occurs throughout the placenta. The dysregulation of transcripts involved in metabolic
283 or developmental processes suggests that GPCMV infection reprograms gene expression
284 throughout the decidua and placenta in ways that could be harmful to fetal development.

285 Gene expression changes in the GPCMV-infected microenvironment

286 GPCMV transcripts are polyadenylated and spatial transcriptomes that contained viral
287 reads were identified in all six samples of GPCMV-infected placenta (**Fig. 5**). To determine how
288 GPCMV affects transcription in infected cells and cells in their immediate vicinity, we compared

289 the results of *gp3*-specific RNAscope with the number of GPCMV reads that were detected per
290 transcriptome (**S2 and S6 Figs.**). Spots that contained more than one hundred viral reads
291 (N=99) colocalized with *gp3*+ cells in the serial tissue section and were annotated as GPCMV-
292 infected. Sample 2395B1 was excluded from this analysis because it lacked spatial
293 transcriptomes that contained more than one hundred viral reads and *gp3*-positive cells. Spots
294 that were located within 110 μm of GPCMV-infected cells were classified as part of the GPCMV-
295 infected microenvironment (N=285) for this differential gene expression analysis. In total, 384
296 spatial transcriptomes from GPCMV-infected placentas were compared with 1148 spatial
297 transcriptomes from the mock-infected tissue sections that were similarly located in the placenta
298 **(Fig. S6)**. Most spatial transcriptomes included in this analysis had been assigned to either the
299 placental stem and junctional zone or the non-capillarized syncytium clusters (**Fig. 6a**).

300 **Figure 5. GPCMV-infected cells are detected in spatial transcriptomes.**
301 SpaceRanger was used to map reads to the GPCMV genome and spatial
302 transcriptomes that contained viral transcripts were identified. (**A**) The number of
303 GPCMV-specific reads in each transcriptome was plotted by sample identifier. GPCMV-
304 infected samples are noted in red, and the data was colored by the viral read count. (**B**)
305 Sequencing data was overlaid onto an image of a GPCMV-infected sample (2421A).
306 Spots were colored based on GPCMV-read count as in (A). (**C**) For differential gene
307 expression analyses, transcriptomes that contained >100 GPCMV reads were defined
308 as “infected” (blue) and any spot within 100 μM was classified as in the GPCMV-infected
309 microenvironment (red).

310 **Figure 6. Chemokine and T cell-associated transcripts are upregulated in or near**
311 **GPCMV-infected cells.** Gene expression was compared between spatial
312 transcriptomes that contained ≥100 GPCMV reads or were within 110 μm of infected
313 cells and a comparable area in mock-infected tissue. **(A)** Bar graph illustrating the

314 cluster assignments for the two groups of transcriptomes that were compared in this
315 analysis. (**B**) Transcript abundance illustrated by volcano plot, highlighting transcripts
316 with chemokine activity (GO:0008009). (**C**) Violin plots displaying the expression of
317 select chemokine transcripts or transcripts related to a cytotoxic immune response in
318 individual transcriptomes. (**D**) g:Profiler was used for functional enrichment analysis to
319 identify terms that are enriched among the transcripts that are differentially regulated by
320 GPCMV infection. Select gene ontology terms are highlighted on a modified Manhattan
321 plot.

322 448 guinea pig transcripts were upregulated in or near GPCMV-infected cells and 530
323 were downregulated (≥2-fold change, $p \leq 0.05$, **Fig. 6b**). Gene ontology analysis revealed a
324 transcriptional signature indicative of immune activation in the GPCMV-infected tissues (**Fig.**
325 **6c**). Notably, the inflammatory response to GPCMV infection appears to be predominantly
326 driven by chemokine signaling. 16 of 18 chemokine transcripts that were enriched in or near
327 GPCMV infected cells were upregulated, including multiple chemokines that signal through
328 Cxcr3 and several chemokines (*Ccl2*-like [LOC100717552], *Ccl3*-like [LOC100734903 and
329 LOC100735187], and *Ccl15*-like [LOC101788094]) that may be unique to guinea pigs (**Fig. 6b**).
330 67 transcripts involved in leukocyte activation (GO:0045321), including markers of a cytotoxic
331 immune response such as *Cd3d*, *Cd8a*, and granzyme transcripts, were also more highly
332 expressed at sites of GPCMV infection. Cytokines that are associated with acute placental
333 infection (e.g. IL-1β, TNFα, IL-6, and IL-8) were not differentially regulated by GPCMV.
334 Similarly, while numerous interferon stimulated gene transcripts (e.g. *Isg15*) were upregulated
335 by infection, transcripts encoding interferons were not affected by GPCMV infection.
336 Cumulatively, spatial transcriptomics resolved direct and indirect effects of GPCMV infection in
337 the placenta and has revealed the central role of chemokine signaling in the GPCMV-infected
338 placenta.

339 # Discussion

340 Placental infection plays a central role in CMV pathogenesis during pregnancy. In this
341 study, we used ST to investigate how GPCMV affects gene expression at the maternal-fetal
342 interface. With its 55-μm spot resolution, the Visium Spatial Gene Expression Platform enabled
343 the most detailed analysis of transcription in the guinea pig placenta and decidua to date,
344 revealing how infection impacts transcription in infected cells and their immediate
345 microenvironment and illuminating how regions of the placenta are affected by the virus when
346 not directly infected.

347 Research in primary trophoblasts, tissue explants, and organoids has provided insights
348 into how HCMV affects the maternal-fetal interface, but these models have notable limitations
349 [18, 20, 25, 26, 47, 48]. During *in vitro* experiments, placental cells or tissue explants are
350 generally exposed to high infectious doses of virus by non-physiologic routes. Samples are
351 analyzed within days of the initial infection, and the resulting data may reflect features of the
352 innate host response to HCMV. Bulk RNA seq experiments have found that HCMV elicits
353 markedly different transcriptional responses from decidua and placenta [20, 26]. Moreover, first
354 and third trimester trophoblasts and tissue explants are differentially susceptible and responsive
355 to HCMV infection [5, 26, 49, 50]. Thus, how CMV infection can cause placental injury likely
356 depends upon when infection occurs during gestation.

357 Clinically, HCMV causes chronic placental infections that are characterized by focal
358 lesions and a heterogeneous population of maternal and fetal leukocytes respond to infection [4,
359 10]. This complexity cannot be easily modeled *in vitro*, but studying samples of infected
360 placenta collected after congenital infections presents its own challenges. Unlike Zika or rubella
361 viruses, primary HCMV infection does not present with diagnostic clinical signs (e.g. rash),
362 molecular methods must be used to confirm infection during pregnancy, most cases are not

363 identified until after birth. Sample heterogeneity further complicates the analysis of clinical
364 samples. For example, ST was used to study placentas collected after SARS-Cov-2 infection
365 during pregnancy [51]. Most of nine samples analyzed did not contain virus that could be
366 detected by qRT-PCR, *in situ* hybridization, or ST. The highest viral loads and most significant
367 infection-associated changes in gene expression were found in two placentas recovered after
368 intrauterine fetal demise at significantly different times in pregnancy (22.3 versus 35.0 weeks).
369 Experimental studies in animal models thus play an important role in revealing how CMV and
370 other viral infections can affect the maternal-fetal interface.

371 Guinea pigs have long been used for preclinical CMV vaccine development, but the
372 limited availability of species-specific reagents has been a barrier to more sophisticated studies
373 of CMV pathogenesis [52]. Species-agnostic next generation sequencing technology has
374 revolutionized discovery science in guinea pigs and other unconventional animal models. For
375 example, scRNA-Seq revealed that naked mole-rats, a hystricomorph rodent like the guinea pig,
376 lack conventional natural killer cells [53]. We have previously used bulk RNA-seq to examine
377 how guinea pig amniotic epithelial cells respond to infection *in vitro* and assess how primary
378 GPCMV infection during the embryonic period or after mid-gestation differentially affect the
379 placenta [38, 43]. However, bulk RNA-seq and most other conventional gene expression
380 analyses quantify transcript abundance in tissue homogenates. This effectively averages
381 transcript abundance across numerous cell types and states. ST enables gene expression
382 analysis at a near single-cell resolution while preserving cellular location in the tissue of interest
383 [54]. While the fresh-frozen Visium Spatial Gene Expression workflow is not reliant on species
384 specific reagents, the 55-μm resolution of each spatial transcriptome is a limitation of the
385 technology. Depending on the cellular density in tissue being analyzed, each spatial
386 transcriptome reflects the RNA content of one to ten cells. Computational approaches have
387 been developed that can infer the cellular composition within spots, as demonstrated by recent

388 studies that used sc- or snRNA-Seq datasets to study the human maternal-fetal interface [51,
389 55]. While cell atlases have been developed for the human and mouse placenta, a similar
390 resource has yet to be developed for the guinea pig and an automated cell type classification
391 was not done in this study. [56-59]

392 This study revealed that GPCMV infection dysregulates more transcripts in the decidua
393 and junctional zone than in the labyrinth or non-capillarized syncytium. HCMV antigens and
394 DNA are more frequently detected in decidua than in placenta, but GPCMV is only sporadically
395 detected in the decidua by *in situ* hybridization at 21 dpi (**Fig. S1**) [38, 60]. Additional
396 experiments are necessary to assess whether GPCMV infects the decidua at earlier times in
397 infection and resolves. One observation from gene set enrichment analysis was that GPCMV
398 infection downregulates lipid metabolism and transport in the maternal-fetal interface. Fetal
399 development and growth are dependent upon the regulated transport of maternal nutrients,
400 including fatty acids, across the placenta and maternal hyperlipidemia is typical during a healthy
401 pregnancy [61, 62]. Abnormal maternal lipid levels are observed during pregnancy-induced
402 hypertension, preeclampsia, and preterm birth [63-65]. At a cellular level, DNA viruses hijack
403 lipid metabolism pathways to promote replication, and HCMV infection promotes fatty acid
404 synthesis and modifies cholesterol synthesis and trafficking *in vitro* [66-70]. Given that ZIKV
405 infection also perturbs lipid homeostasis in the placenta, altered lipid metabolism may a
406 mechanism by which viruses cause placental insufficiency [71].

407 Placental dysfunction and adverse fetal outcomes can be caused by interferon signaling
408 and other inflammatory responses to infection [8, 72]. Infection is a leading cause of preterm
409 birth, and the acute inflammatory responses to ascending bacterial infection involves cytokines,
410 including IL-1β, IL-6, IL-8, and TNF-α, that are normally upregulated during parturition [73].
411 Polyinosinic:polycytidylic acid (Poly I:C), a synthetic analog of the viral pathogen associated
412 molecular pattern double-stranded RNA, can affect placental and fetal development in mice and

413 rats depending upon the dose, route of administration, and the timing of treatment during
414 pregnancy [reviewed in [74]]. Experiments in *Ifnar*-transgenic mice have demonstrated that fetal
415 growth restriction and resorption can be caused by Type I interferon signaling that occurs in the
416 Zika virus (ZIKV)-infected fetus and placenta [27, 75, 76]. In humans, Aicardi–Goutières (AGS)
417 syndrome, a rare inherited disease characterized by dysregulated Type I interferon production,
418 can present during pregnancy with ultrasound findings reminiscent of congenital infections [77].

419 Multiple studies have found that cCMV causes proinflammatory cytokines to accumulate
420 in amniotic fluid, and elevated CXCL10 levels are a biomarker of congenital infection [22-24].
421 CMV infection also upregulates *CXCL10* transcription in tissue explants, amniotic epithelial
422 cells, and decidual organoids *in vitro* [20, 26, 43]. Elevated amniotic fluid concentrations of
423 CXCL10 also occurs during chronic chorioamnionitis and maternal anti-fetal rejection; the
424 chemokine may drive T cell recruitment to the placenta and/or fetal membranes [78-80]. Bulk
425 RNA-Seq found that *Cxcl10* is upregulated in the GPCMV-infected placenta, and ST confirmed
426 this finding while also revealing that a broad mix of chemokines are upregulated in the
427 microenvironment around GPCMV-infected cells [38]. Curiously, while individual interferon
428 stimulated genes are upregulated during placental GPCMV infection, interferon transcripts were
429 not regulated by infection. Interestingly, one study found no association between CXCL10
430 concentrations and the detection of HHV6, parvovirus B19, or Epstein-Barr virus in amniotic
431 fluid [23]. Nonhuman primate studies also indicate that the inflammatory response to CMV may
432 be distinct from other viral causes of placental and congenital infections such as ZIKV [81, 82].

433 Primates and rodents diverged 100 million years ago, and the cytomegaloviruses have
434 been cospeciating with their hosts ever since [83, 84]. The species-specificity of HCMV
435 precludes the direct study of the virus in animal models, and while *in vivo* experiments using
436 closely related primate and guinea pig cytomegaloviruses can reveal how infection affects the
437 placenta under controlled experimental conditions, virus and host-specific immune adaptations

438 could limit the translatability of these studies to humans. For example, GPCMV-specific
439 adaptations to its host's immune system include the convergent evolution of class I MHC mimics
440 and a unique viral chemokine, *gp1* [85, 86]. Guinea pigs and other caviomorph rodents have a
441 unique population of mononuclear cells, Kurloff cells, with natural killer (NK) cell activities [87].
442 While direct functional comparisons to human or mouse decidual NK cells have yet to be
443 completed, the abundance of circulating Kurloff cells is regulated by estrogen and the cells
444 localize to the placenta and uterus in pregnant animals [88, 89]. While this study and our
445 previous bulk RNA-seq of the guinea pig placenta provide valuable insights into the biology of
446 the maternal-fetal interface in guinea pigs, more extensive studies of placental gene expression
447 and guinea pig immunity are merited to support the use of the rodent as a comparative model
448 for human gestation [38].

449 Materials and Methods.

450 Ethics Statement.

451 All animal procedures were conducted in accordance with protocols approved by the
452 Institutional Animal Care and Use Committee (IACUC) at the University of Minnesota,
453 Minneapolis (Protocol IDs: 1810-36403A and 2106-39180A). Experimental protocols and
454 endpoints were developed in strict accordance to the National Institutes of Health Office of
455 Laboratory Animal Welfare (Animal Welfare Assurance #A3456-01), Public Health Service
456 Policy on Humane Care and Use of Laboratory Animals, and United States Department of
457 Agriculture Animal Welfare Act guidelines and regulations (USDA Registration # 41-R-0005)
458 with the oversight and approval of the IACUC. Guinea pigs were housed in a facility maintained
459 by the University of Minnesota Research Animal Resources, who were accredited through the
460 Association for Assessment and Accreditation of Laboratory Animal Care, International

461 (AAALAC). All procedures were conducted by trained personnel under the supervision of
462 veterinary staff.

463 Infection of Pregnant Guinea Pigs and Tissue Collection.

464 GPCMV seronegative, pregnant guinea pigs were mock- or GPCMV- infected as
465 previously described [38]. Briefly, two- to three-month-old strain 2 females were housed with
466 strain 2 males until pregnancy could be confirmed by palpation. At this point, the strain 2 male
467 was replaced with a strain 13 male, who remained with the female until three days postpartum
468 to establish a second, timed pregnancy [42]. Progesterone ELISA and/or palpation was used to
469 confirm the second pregnancy. At 35 days dGA, guinea pigs were injected subcutaneously into
470 the scruff of the neck with 0.5 mL of GPCMV-containing PBS ($2x10^5$ PFU, SG13J2) or PBS
471 alone [43]. Blood and plasma were collected from dams every seven days post-infection (dpi)
472 until the animals were euthanized at 21 dpi. Several dams also received intraperitoneal (IP)
473 injections of 1.5 mg of rat IgG (2 mg/mL in PBS) at days 0, 7, and 14 post-infection or an IP
474 injection of 80 mg of Hypoxyprobe 1 (pimonidazole HCl) dissolved in PBS that was administered
475 90 minutes before the animal was euthanized (Supplementary Table 1). During tissue collection,
476 the uterus was dissected, the decidua gently separated from the uterus, and each placenta was
477 halved. One half of each placenta was embedded in optimal cutting temperature (OCT)
478 compound and flash frozen in isopentane chilled with a dry ice ethanol bath. A portion of the
479 remaining tissue was frozen at -80ºC for DNA extraction and viral load quantification.

480 Screening Placentas for GPCMV Infection and Fetal Sex.

481 DNA was extracted from placentas using the DNeasy Blood and Tissue Kit (Qiagen).
482 The abundance of GPCMV genomes in the tissue was quantified by ddPCR using primers and
483 probes specific to *GP54* and the Bio-Rad QX200 system as previously described [43]. A
484 multiplexed endpoint PCR assay that targets *Sry* (Y-specific) and *Dmd* (X-specific) was used to

485 determine the sex of each placenta [44]. The location of GPCMV-infected cells in placenta was
486 determined using an RNAscope® assay specific to the viral transcript *gp3* (Probe V-CavHV-2-
487 gp3) [38]. Fresh-frozen tissue was prepared for single-plex RNAscope® 2.5 assays as
488 described in technical note 320536-TN Date 11112016. 10-µm sections of placenta were
489 mounted onto Superfrost Plus slides (ThermoFisher), fixed using 4% paraformaldehyde, and
490 dehydrated by sequential immersion in 50%, 70%, and 100% ethanol. After the slides were
491 dried, the tissue was treated with RNAscope® hydrogen peroxide and Protease IV. The slides
492 were then stained with RNAscope® 2.5 HD Detection Reagent – RED (322360-USM Rev. Date
493 11052015) as previously described (9).

494 Spatial Transcriptomics

495 To optimize on-slide cDNA synthesis for ST, mock-infected placentas collected at 42
496 and 56 dGA were analyzed using Tissue Optimization Slides and Reagents (10x Genomics,
497 PN-1000194). Blocks of frozen placenta were trimmed with the goal of including the main
498 placenta, placental stem, and decidua on each capture area. 10 µm tissue sections were placed
499 onto seven of the eight capture areas on the tissue optimization slide (CG000240 Rev B).
500 Tissue was fixed with methanol, H&E stained, and imaged with a Huron TissueScope LE
501 (CG000160 Rev A). For tissue permeabilization and fluorescent cDNA synthesis, capture areas
502 were incubated with Permeabilization Enzyme for times that ranged from 3 to 30 minutes
503 (CG000238 Rev C). After reverse transcription, slides were imaged with a Nikon Eclipse
504 fluorescent microscope. An 18-minute permeabilization time was selected for ST experiments
505 based on the quality of the fluorescent signal. Irrespective of the permeabilization time, more
506 signal was observed in the main placenta than in the subplacenta, placental stem, or decidua.

507 Five GPCMV-infected and six control placentas were sectioned onto the twelve capture
508 areas of three Visium Spatial Gene Expression Slides. These tissues originated from three

509 GPCMV- and three mock-infected dams and were a mixture of males and females. Blocks were
510 roughly trimmed to 6.5x6.5 mm^2 so that a similar region of interest would be included in each
511 capture area and, for GPCMV-infected samples, infected cells would be included in the capture
512 areas. One GPCMV-infected placenta (2395B) was divided and sectioned onto two capture
513 areas. The slides were fixed, H&E stained, and imaged with a Huron TissueScope LE. The
514 tissue was then permeabilized for 18 minutes and cDNA synthesis, amplification, and
515 sequencing library preparation was completed using the manufacturer recommended protocol
516 (CG000239 Rev C). Visium libraries were combined and sequenced on a single Illumina
517 NovaSeq S4 lane (2 x 150 PE run format). Sequencing results are summarized in
518 Supplementary Table 1. A median of $2.2X10^8$ reads per capture area (range $1.0X10^8$ to
519 $6.9X10^8$) and $7.3X10^4$ reads per spatial transcriptome (range $3.3X10^4$ to $1.8X10^5$) were
520 sequenced. Sequencing data has been uploaded to the Gene Expression Omnibus (Series
521 GSE303764, https://www.ncbi.nlm.nih.gov/geo/query/acc.cgi?acc=GSE303764).

522 Data analysis

523 To analyze ST data, a custom reference sequence that combined the guinea pig
524 genome (Cavpor3.0, GCF_000151735.1, Annotation Release 103), the GPCMV genome (strain
525 22122, NC_020231), and a list of Y chromosome transcripts, was prepared [90, 91]. Space
526 Ranger (10x Genomics, version 1.3.0) was used to process the raw Illumina sequencing data.
527 Space Ranger outputs were uploaded to *Partek® Flow®* software (v10.0). Reads that aligned to
528 the GPCMV genome from each sample of infected placenta were visualized with Geneious
529 (v11.1.5). Each capture area was manually examined and 927 spatial transcriptomes that were
530 located under folded or visibly damaged tissue were excluded from downstream analyses. For
531 graph-based clustering, data from the remaining 33,687 spots was filtered to the 3000 most
532 variable features, normalized with SCTransform, and batch corrected with Seurat3 integration
533 [92, 93]. 50 principal components were used for graph-based clustering and data presentation

534 by Uniform Manifold Approximation and Projection (UMAP) dimensional reduction. Sensitivities
535 from 0.3 to 1.0 were evaluated using the Louvain clustering algorithm. Higher resolution settings
536 predictably identified more clusters but also resulted in considerable variation in the number of
537 spatial transcriptomes assigned to each cluster across the twelve samples. A resolution setting
538 of 0.5 was selected for subsequent analyses. The data was further refined by excluding 1018
539 spatial transcriptomes that were located at the edges of tissue sections and combining several
540 clusters. Cluster-specific biomarkers were identified using Partek Flow's "compute biomarker"
541 tool. This algorithm compared the expression of features in each cluster with the expression
542 observed in all other clusters combined using student's t-tests.

543 To identify host transcripts that were differentially regulated by GPCMV infection, the
544 abundance of all transcripts that were detected in >0.1% of spatial transcriptomes was
545 normalized to counts per million plus one and $\log_2$ transformed. Differentially regulated
546 transcripts were identified by gene-specific analysis (GSA). In one analysis, transcripts that
547 were differentially regulated by infection were identified in each of the previously identified
548 clusters. In a second analysis, spatial transcriptomes that contained ≥100 GPCMV transcripts
549 and every spatial transcriptome within 110 μm were defined as the GPCMV-infected
550 microenvironment. Transcript abundance was compared with similar area that was manually
551 selected from mock-infected tissue sections, and 384 spatial transcriptomes from GPCMV-
552 infected placentas were compared with 1148 spatial transcriptomes from control tissue. For both
553 workflows, functional enrichment analyses on differentially regulated transcripts (twofold or
554 more, $p < 0.05$) were completed using g:Profiler [46].

555 Acknowledgements

556 This work was supported by the National Institutes of Health's National Center for Advancing
557 Translational Sciences, which provided funding for the Biorepository and Laboratory Services

558 Team, and the resources and staff at the University of Minnesota University Imaging Centers
559 (SCR_020997) and the Genomics Center (https://genomics.umn.edu). The content of this article
560 is solely the responsibility of the authors and does not necessarily represent the official views of
561 the National Institutes of Health's National Center for Advancing Translational Sciences.

562 **Competing interests.**

563 The authors have no competing interests to declare.

564

Figure 1.

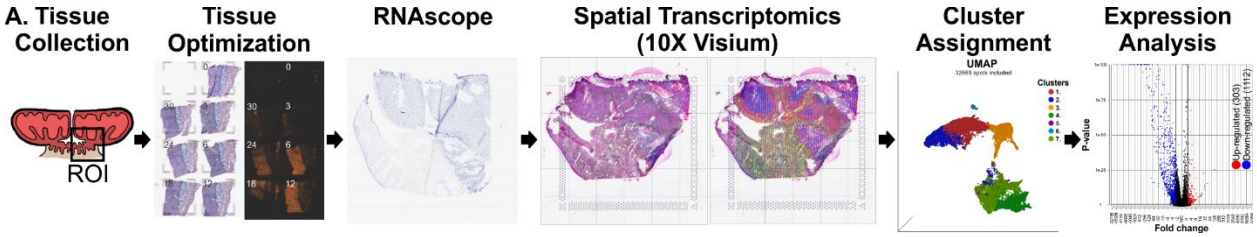
A. Tissue Collection
ROI
Tissue Optimization
RNAscope
Spatial Transcriptomics (10X Visium)
Cluster Assignment
UMAP
Clusters
Expression Analysis
P-value
Fold change
Up-regulated (303)
Down-regulated (1112)

570 **Figure 2.**

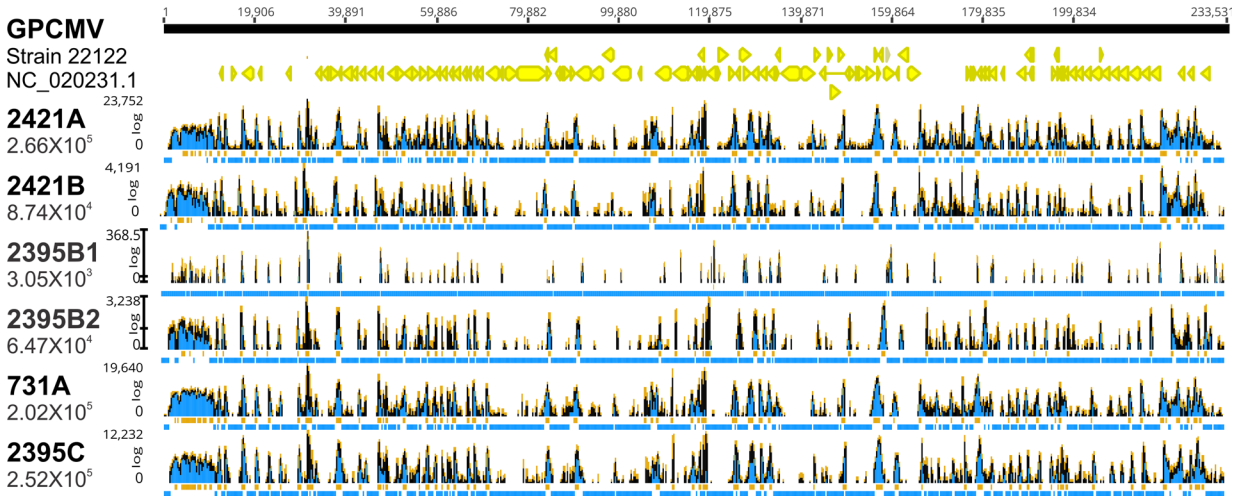

571

572

Figure 3.

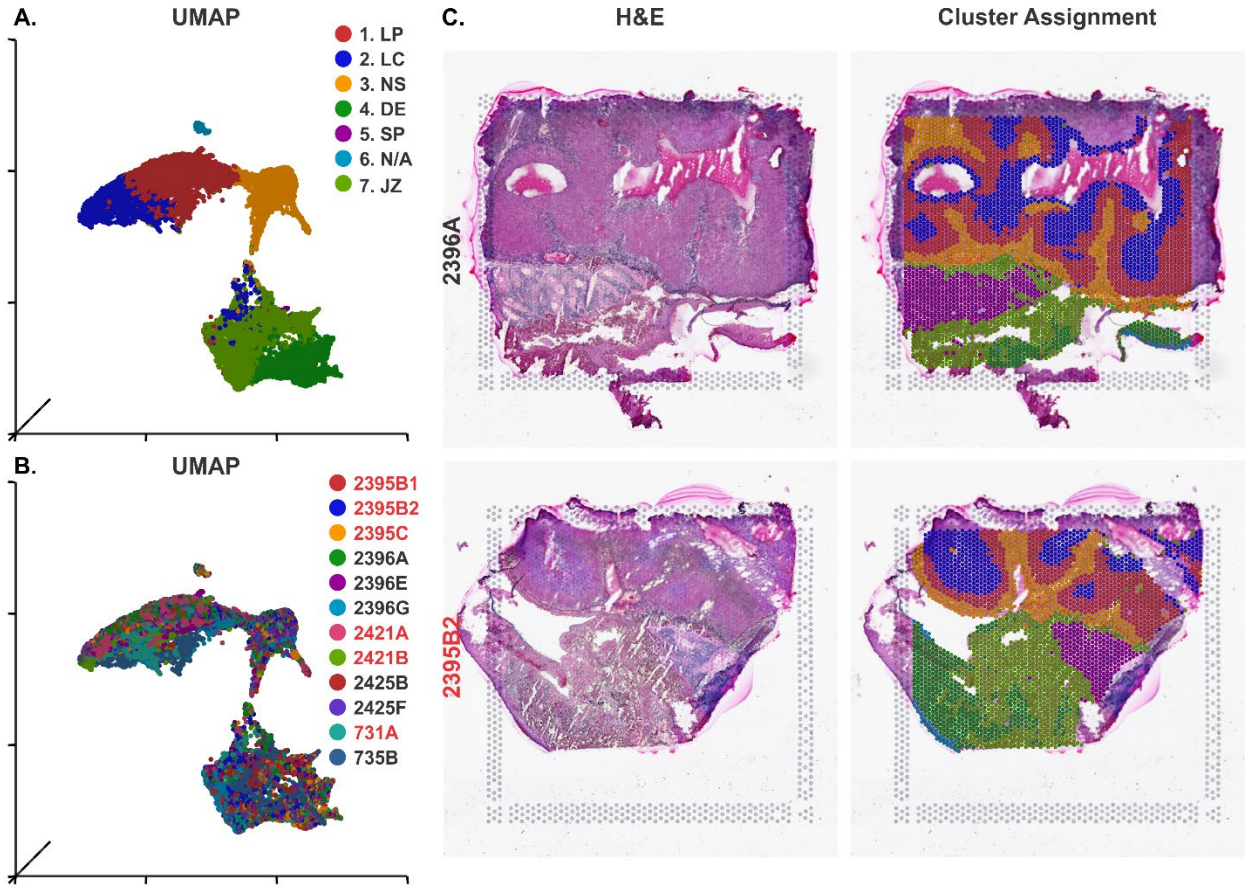
A.
UMAP
1. LP
2. LC
3. NS
4. DE
5. SP
6. N/A
7. JZ
B.
UMAP
2395B1
2395B2
2395C
2396A
2396E
2396G
2421A
2421B
2425B
2425F
731A
735B
C.
H&E
Cluster Assignment
2396A
2395B2

577 **Figure 4**.

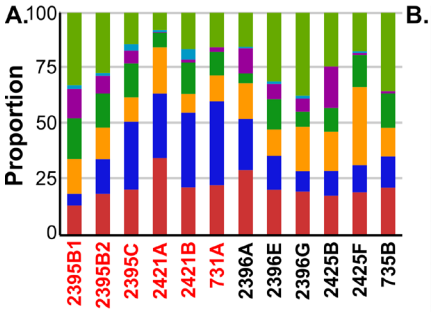

Cluster	# Spots (CMV/Mock)	Up-Regulated	Down-Regulated
1. LP	3508 / 3685	42	87
2. LC	3868 / 2442	43	61
3. NS	2247 / 3152	48	82
4. DE	2121 / 1706	303	1112
5. SP	859 / 1168	100	134
6. N/A	278 / 110	ND	ND
7. JZ	3054 / 4420	281	585

578

579

580 **Figure 5.**

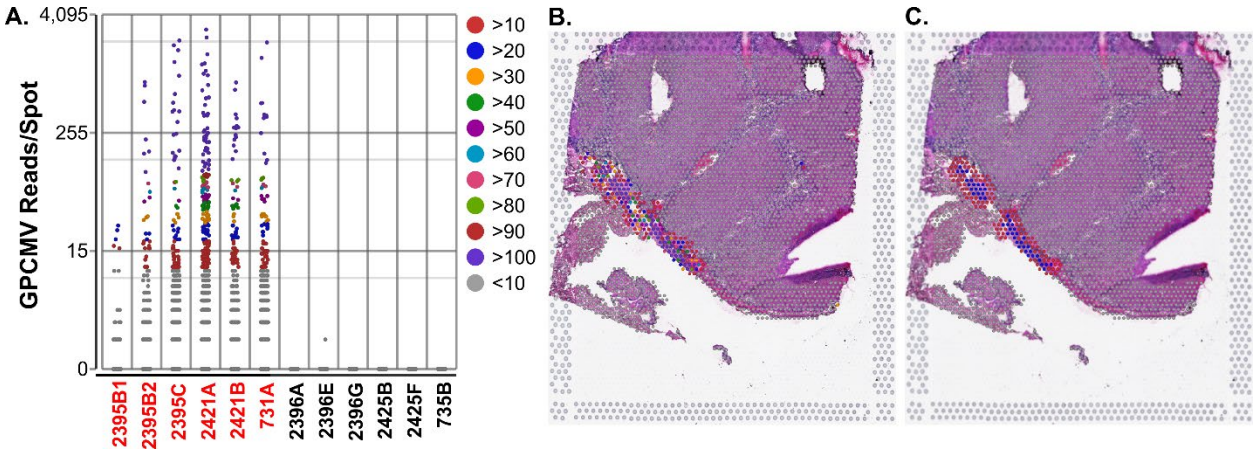

581

582

583 **Figure 6.**

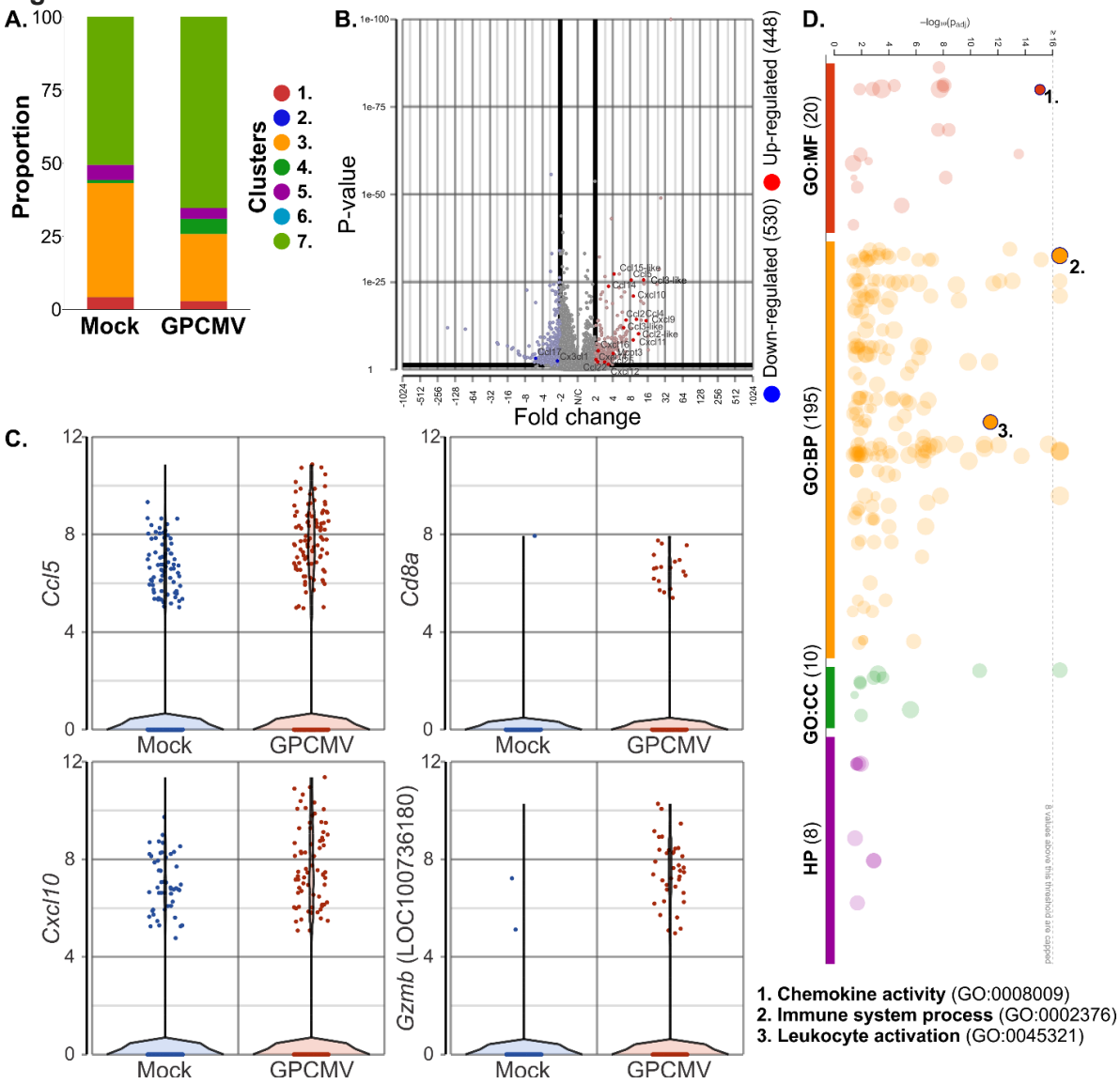

584

585

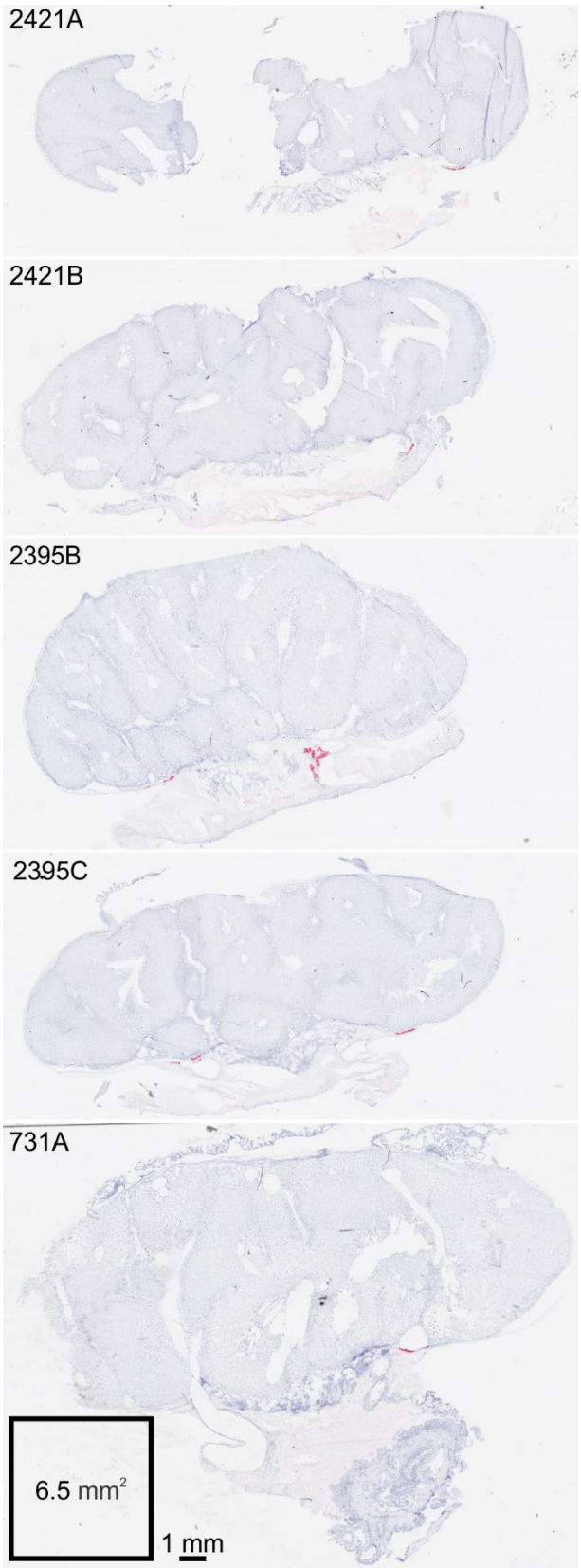

Supporting Information.

S1 Figure. GPCMV-specific RNAscope. Fresh-frozen, GPCMV-infected placentas were cross-sectioned and stained with a RNAscope assay that detects the viral transcript *gp3* (red). Scans of the five infected placentas that were selected for ST are shown.

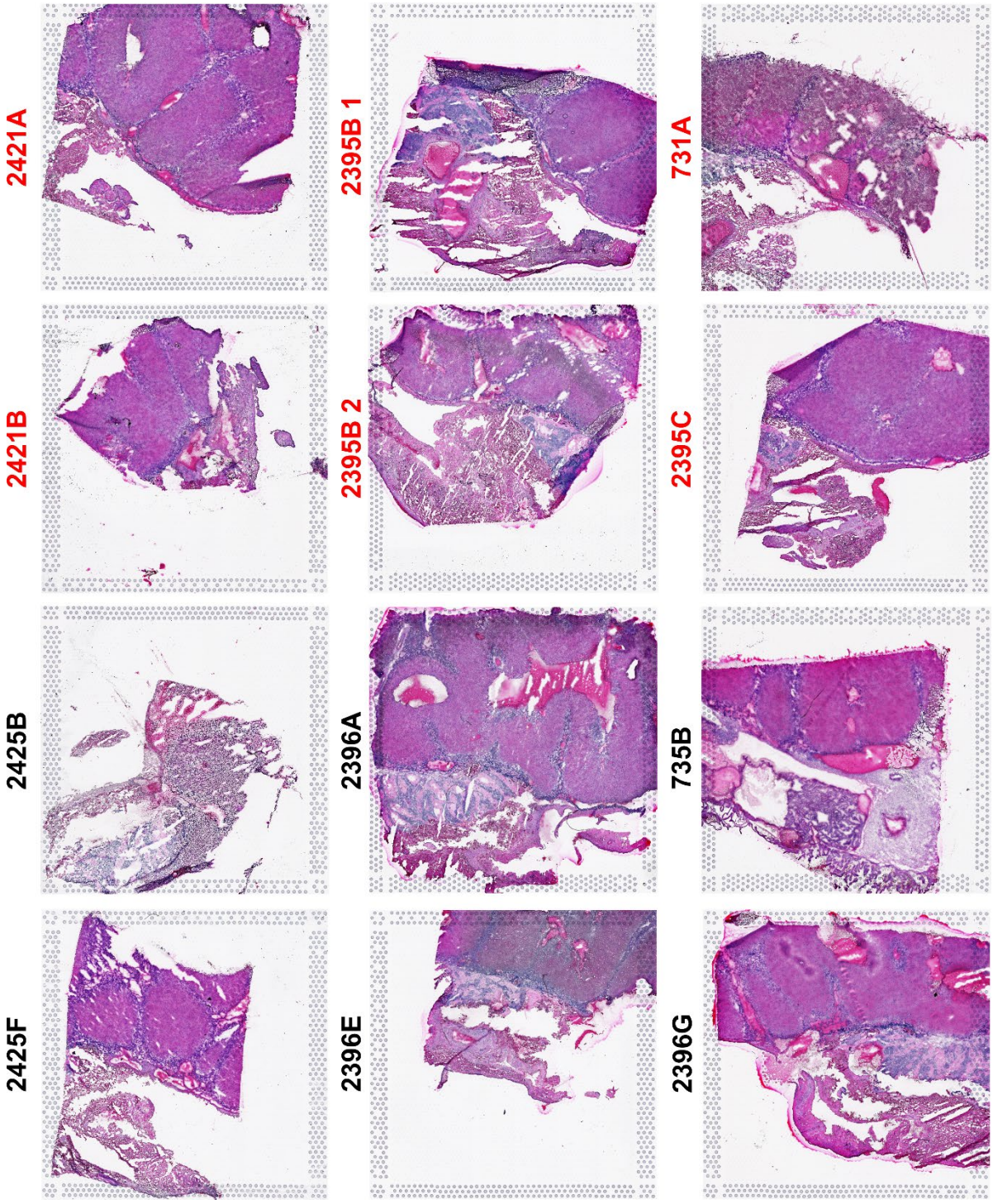

S2 Figure. Hematoxylin and eosin-stained guinea pig placentas. GPCMV- (**Red**, N=5) and mock-infected placentas (N=6) were trimmed and sectioned onto twelve capture areas. The Visium Spatial Gene Expression Slides were H&E stained and imaged. The images were cropped to each capture area's fiducial frame and oriented so that the main placenta is up and decidua down.

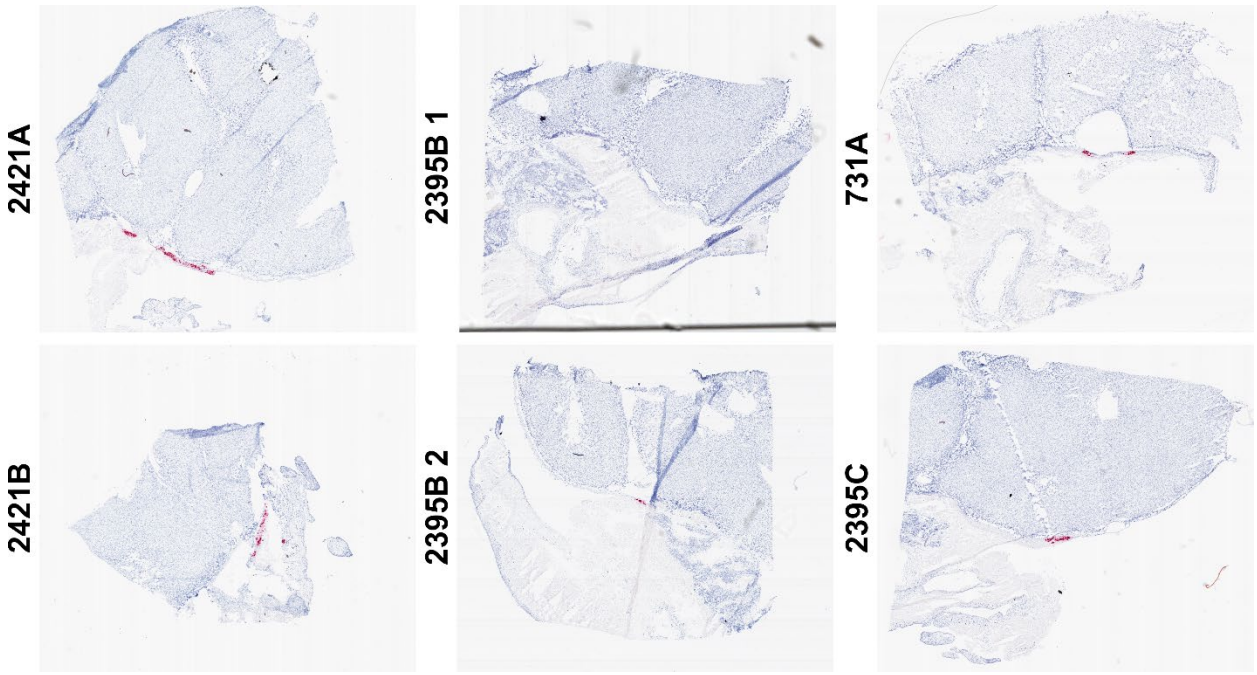

S3 Figure. GPCMV-specific RNAscope of trimmed placentas. Placentas were trimmed to accommodate the 6.5X6.5 mm^2 Visium capture area. After tissue was sectioned on the Visium Gene Expression Slides, the serial section from each sample was used for gp3-specific RNAscope (red) to confirm that infected cells had been placed within each capture area.

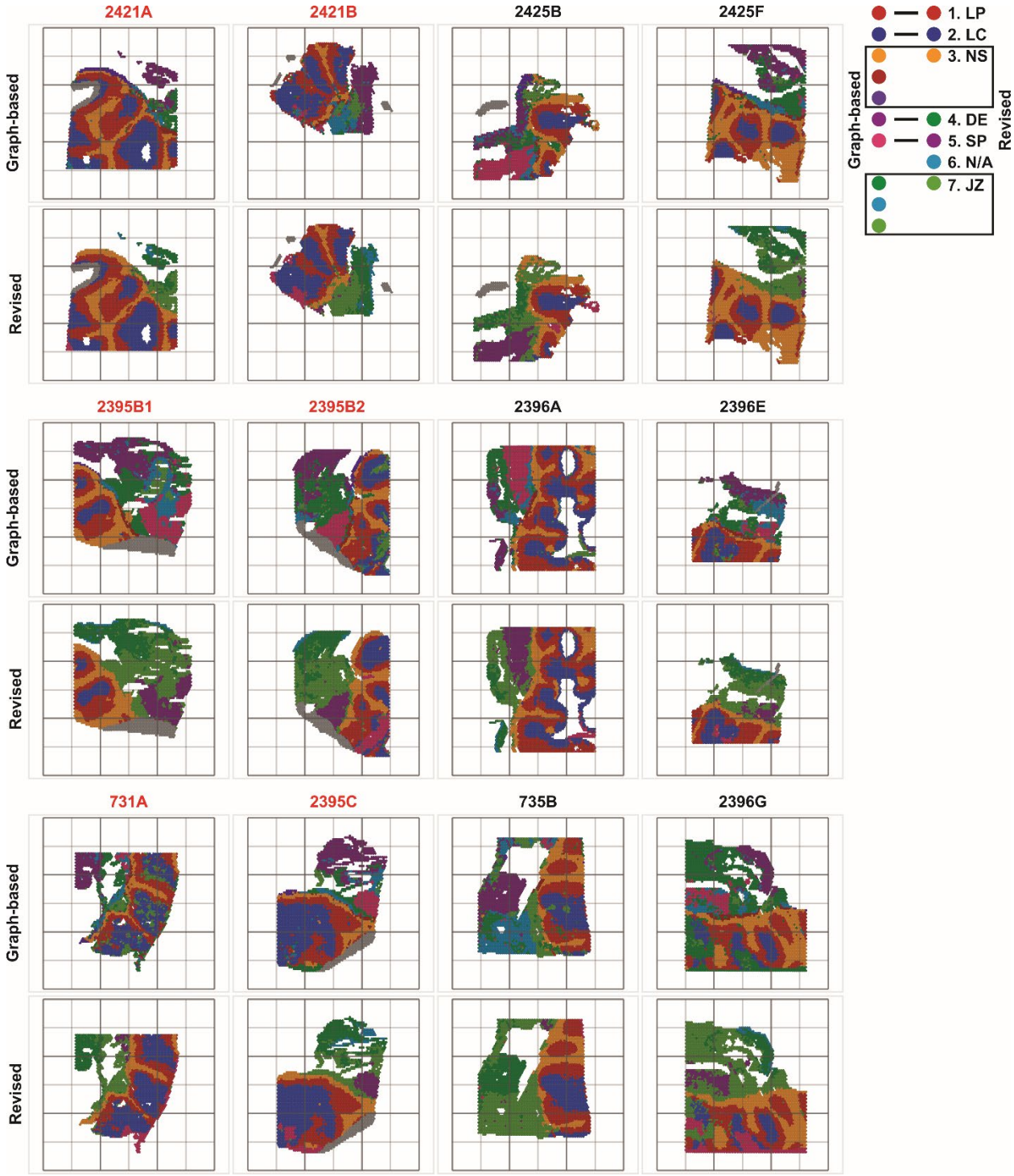

S4 Figure. Spatial transcriptomes cluster by anatomic region. Graph-based clustering assigned spatial transcriptomes to ten groups. These were further manually refined to seven clusters, which included excluding data under folded tissue sections, near large blood spaces, and combining several smaller clusters into groups representing non-capillarized syncytium and the junctional zone and placenta stem.

614

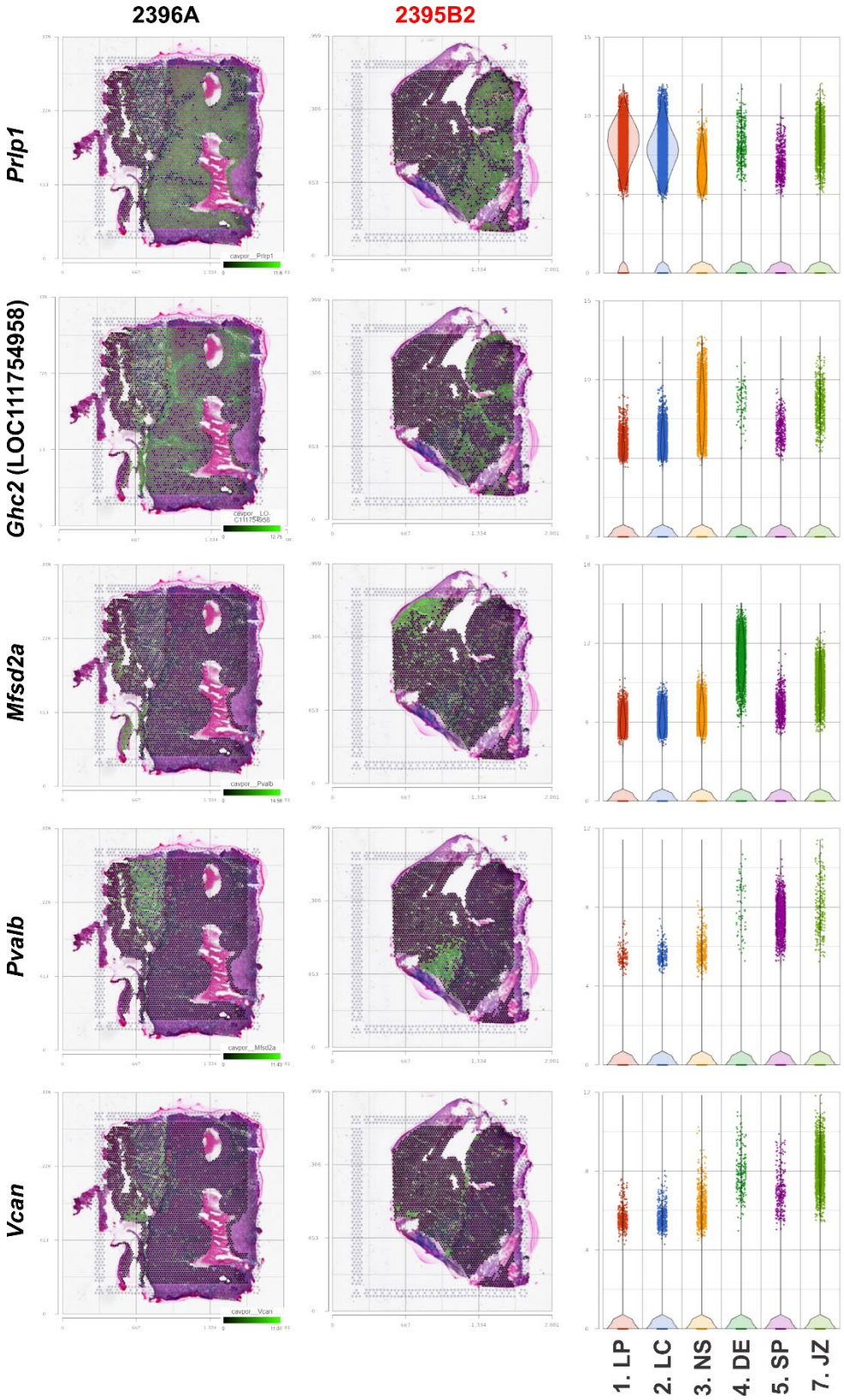

S5 Figure. Biomarker expression in the anatomic regions of the guinea pig placenta. Transcripts were identified that were significantly enriched in each cluster. Gene expression data for select biomarkers was overlaid on two representative sections of placenta such that transcript abundance in each spot is represented by green intensity. Violin pots illustrate the expression of each biomarker in all samples with transcriptomes classified by cluster.

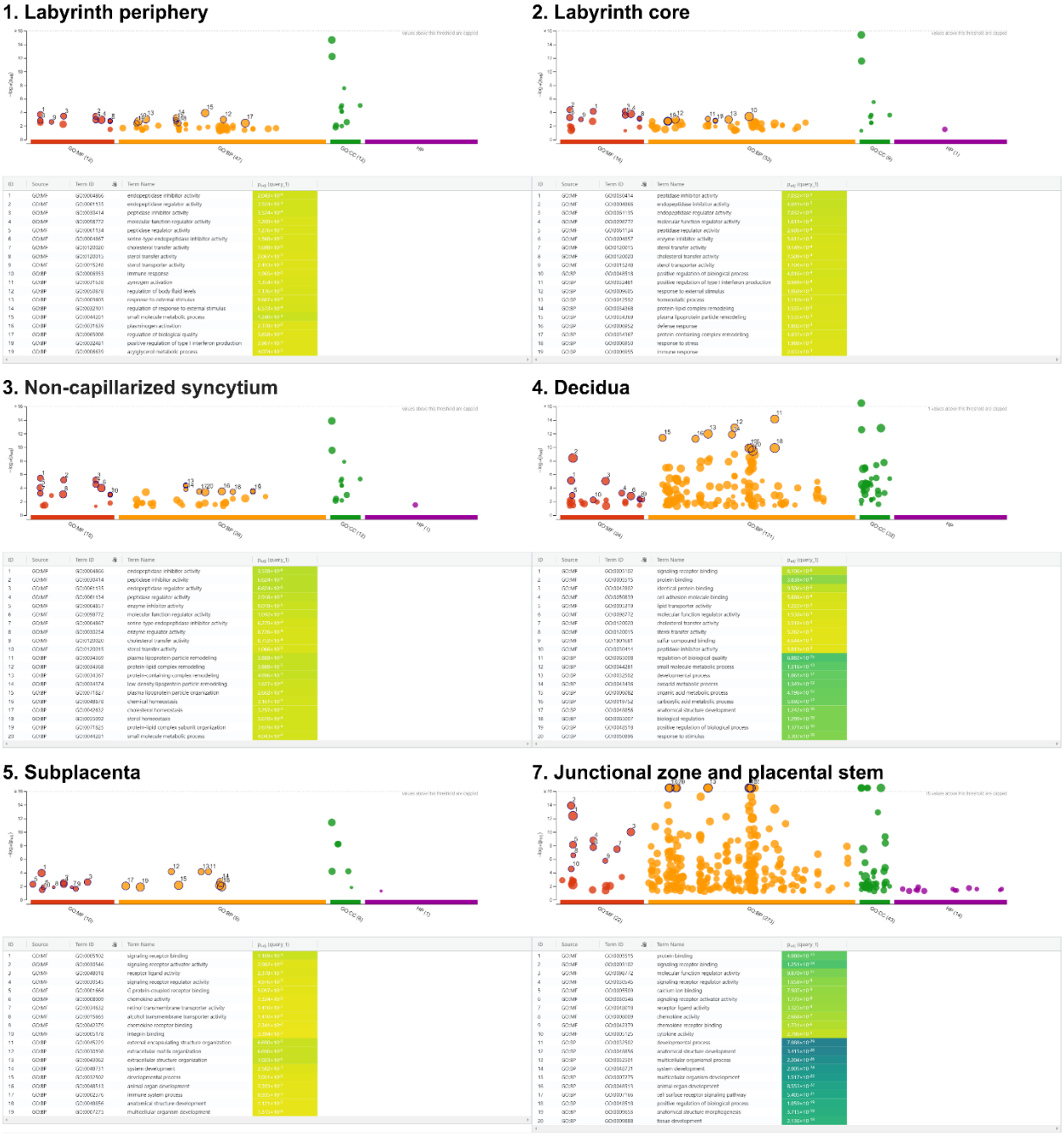

S6 Figure. Functional enrichment analyses reveal pathways dysregulated by GPCMV infection. For each anatomic region of the placenta, transcripts that were significantly up- or down-regulated in GPCMV-infected placenta were identified using GSA. Functional enrichment analyses were done using g:Profiler [46]. Enriched pathways are illustrated by Manhattan plot and the ten most significantly enriched molecular functions and biological processes for each cluster are indicated.

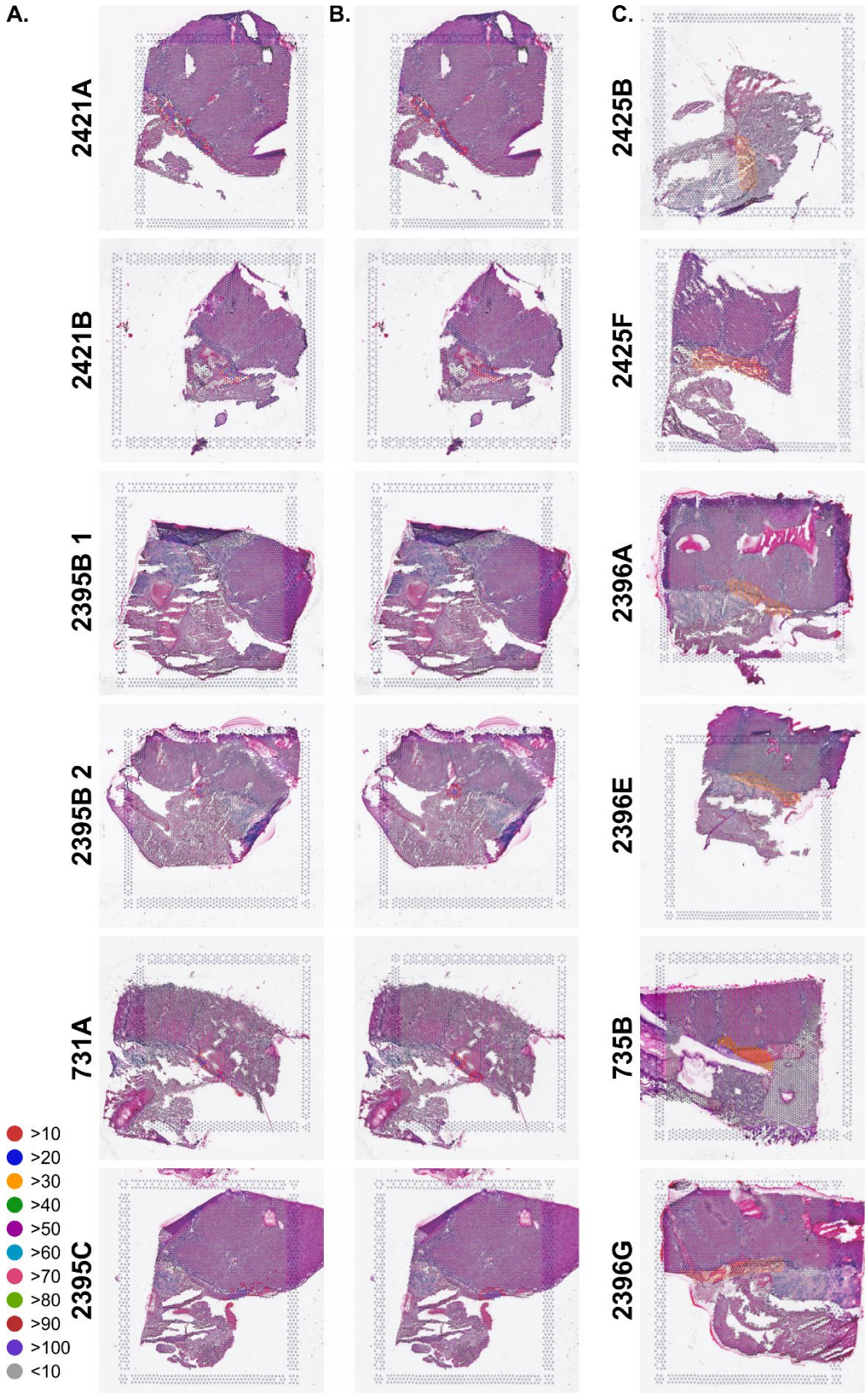
A.
B.
C.
2421A
2421B
2395B 1
2395B 2
731A
2395C
2425B
2425F
2396A
2396E
735B
2396G
>10
>20
>30
>40
>50
>60
>70
>80
>90
>100
<10

653

654 **S7 Figure. Identification of GPCMV-infected cells and their microenvironment in spatial**
655 **transcriptomes.** Transcriptomes that contained GPCMV reads were identified in each capture
656 area. In GPCMV-infected samples, spatial transcriptomes were either colored by the abundance
657 of viral reads or red for >100 reads or blue to designate the microenvironment near infected
658 cells. In mock-infected samples, transcriptomes colored in yellow were selected for the
659 differential gene expression analysis.

660

661 **References**

662 1. Mocarski Jr ES, Shenk T, Griffiths PD, Pass RF. Cytomegaloviruses. In: Knipe DM,
663 Howley PM, editors. Fields virology. 2. 6th ed. Philadelphia, PA: Wolters Kluwer/Lippincott
664 Williams & Wilkins Health; 2013. p. 1960-2014.

665 2. Kenneson A, Cannon MJ. Review and meta-analysis of the epidemiology of congenital
666 cytomegalovirus (CMV) infection. Rev Med Virol. 2007;17(4):253-76. Epub 2007/06/21. doi:
667 10.1002/rmv.535. PubMed PMID: 17579921.

668 3. Megli CJ, Coyne CB. Infections at the maternal-fetal interface: an overview of
669 pathogenesis and defence. Nat Rev Microbiol. 2022;20(2):67-82. Epub 20210825. doi:
670 10.1038/s41579-021-00610-y. PubMed PMID: 34433930; PubMed Central PMCID:
671 PMCPMC8386341.

672 4. Garcia AG, Fonseca EF, Marques RL, Lobato YY. Placental morphology in
673 cytomegalovirus infection. Placenta. 1989;10(1):1-18. Epub 1989/01/01. doi: 10.1016/0143-
674 4004(89)90002-7. PubMed PMID: 2541426.

675 5. Maidji E, Nigro G, Tabata T, McDonagh S, Nozawa N, Shiboski S, et al. Antibody
676 treatment promotes compensation for human cytomegalovirus-induced pathogenesis and a
677 hypoxia-like condition in placentas with congenital infection. Am J Pathol. 2010;177(3):1298-
678 310. Epub 20100722. doi: 10.2353/ajpath.2010.091210. PubMed PMID: 20651234; PubMed
679 Central PMCID: PMCPMC2928963.

680 6. Iwasenko JM, Howard J, Arbuckle S, Graf N, Hall B, Craig ME, Rawlinson WD. Human
681 cytomegalovirus infection is detected frequently in stillbirths and is associated with fetal
682 thrombotic vasculopathy. J Infect Dis. 2011;203(11):1526-33. Epub 2011/05/20. doi:
683 10.1093/infdis/jir121. PubMed PMID: 21592980.

684 7. Pereira L, Petitt M, Fong A, Tsuge M, Tabata T, Fang-Hoover J, et al. Intrauterine
685 growth restriction caused by underlying congenital cytomegalovirus infection. J Infect Dis.

686 2014;209(10):1573-84. Epub 20140107. doi: 10.1093/infdis/jiu019. PubMed PMID: 24403553;
687 PubMed Central PMCID: PMCPMC3997585.
688 8. Yockey LJ, Lucas C, Iwasaki A. Contributions of maternal and fetal antiviral immunity in
689 congenital disease. Science. 2020;368(6491):608-12. Epub 2020/05/10. doi:
690 10.1126/science.aaz1960. PubMed PMID: 32381717.
691 9. Pereira L, Maidji E, McDonagh S, Tabata T. Insights into viral transmission at the
692 uterine-placental interface. Trends Microbiol. 2005;13(4):164-74. doi: 10.1016/j.tim.2005.02.009.
693 PubMed PMID: 15817386.
694 10. Uenaka M, Morizane M, Tanimura K, Deguchi M, Kanzawa M, Itoh T, Yamada H.
695 Histopathological analysis of placentas with congenital cytomegalovirus infection. Placenta.
696 2019;75:62-7. Epub 20190104. doi: 10.1016/j.placenta.2019.01.003. PubMed PMID: 30712668.
697 11. Faure-Bardon V, Magny JF, Parodi M, Couderc S, Garcia P, Maillotte AM, et al.
698 Sequelae of Congenital Cytomegalovirus Following Maternal Primary Infections Are Limited to
699 Those Acquired in the First Trimester of Pregnancy. Clin Infect Dis. 2019;69(9):1526-32. Epub
700 2019/01/01. doi: 10.1093/cid/ciy1128. PubMed PMID: 30596974.
701 12. Fisher S, Genbacev O, Maidji E, Pereira L. Human cytomegalovirus infection of
702 placental cytotrophoblasts in vitro and in utero: implications for transmission and pathogenesis.
703 J Virol. 2000;74(15):6808-20. Epub 2000/07/11. doi: 10.1128/jvi.74.15.6808-6820.2000.
704 PubMed PMID: 10888620; PubMed Central PMCID: PMCPMC112198.
705 13. Zydek M, Petitt M, Fang-Hoover J, Adler B, Kauvar LM, Pereira L, Tabata T. HCMV
706 infection of human trophoblast progenitor cells of the placenta is neutralized by a human
707 monoclonal antibody to glycoprotein B and not by antibodies to the pentamer complex. Viruses.
708 2014;6(3):1346-64. Epub 20140319. doi: 10.3390/v6031346. PubMed PMID: 24651029;
709 PubMed Central PMCID: PMCPMC3970154.
710 14. Tabata T, Petitt M, Zydek M, Fang-Hoover J, Larocque N, Tsuge M, et al. Human
711 cytomegalovirus infection interferes with the maintenance and differentiation of trophoblast

712 progenitor cells of the human placenta. J Virol. 2015;89(9):5134-47. Epub 20150304. doi:
713 10.1128/JVI.03674-14. PubMed PMID: 25741001; PubMed Central PMCID: PMCPMC4403461.
714 15. Halwachs-Baumann G, Wilders-Truschnig M, Desoye G, Hahn T, Kiesel L, Klingel K, et
715 al. Human trophoblast cells are permissive to the complete replicative cycle of human
716 cytomegalovirus. J Virol. 1998;72(9):7598-602. doi: 10.1128/JVI.72.9.7598-7602.1998. PubMed
717 PMID: 9696860; PubMed Central PMCID: PMCPMC110014.
718 16. Pereira L, Tabata T, Petitt M, Fang-Hoover J. Congenital cytomegalovirus infection
719 undermines early development and functions of the human placenta. Placenta. 2017;59 Suppl
720 1:S8-S16. Epub 20170425. doi: 10.1016/j.placenta.2017.04.020. PubMed PMID: 28477968.
721 17. Tabata T, Petitt M, Fang-Hoover J, Rivera J, Nozawa N, Shiboski S, et al.
722 Cytomegalovirus impairs cytotrophoblast-induced lymphangiogenesis and vascular remodeling
723 in an in vivo human placentation model. Am J Pathol. 2012;181(5):1540-59. Epub 20120907.
724 doi: 10.1016/j.ajpath.2012.08.003. PubMed PMID: 22959908; PubMed Central PMCID:
725 PMCPMC3483806.
726 18. Rollman TB, Berkebile ZW, Okae H, Bardwell VJ, Gearhart MD, Bierle CJ. Human
727 Trophoblast Stem Cells Restrict Human Cytomegalovirus Replication. bioRxiv.
728 2023:2023.12.13.571456. Epub 20231214. doi: 10.1101/2023.12.13.571456. PubMed PMID:
729 38168202; PubMed Central PMCID: PMCPMC10760179.
730 19. Okae H, Toh H, Sato T, Hiura H, Takahashi S, Shirane K, et al. Derivation of Human
731 Trophoblast Stem Cells. Cell Stem Cell. 2018;22(1):50-63 e6. Epub 20171214. doi:
732 10.1016/j.stem.2017.11.004. PubMed PMID: 29249463.
733 20. Yang L, Semmes EC, Ovies C, Megli C, Permar S, Gilner JB, Coyne CB. Innate immune
734 signaling in trophoblast and decidua organoids defines differential antiviral defenses at the
735 maternal-fetal interface. Elife. 2022;11:e79794. Epub 20220817. doi: 10.7554/eLife.79794.
736 PubMed PMID: 35975985; PubMed Central PMCID: PMCPMC9470165.

737 21. Goldstein JA, Gallagher K, Beck C, Kumar R, Gernand AD. Maternal-Fetal Inflammation
738 in the Placenta and the Developmental Origins of Health and Disease. Front Immunol.
739 2020;11:531543. Epub 20201113. doi: 10.3389/fimmu.2020.531543. PubMed PMID: 33281808;
740 PubMed Central PMCID: PMCPMC7691234.
741 22. Scott GM, Chow SS, Craig ME, Pang CN, Hall B, Wilkins MR, et al. Cytomegalovirus
742 infection during pregnancy with maternofetal transmission induces a proinflammatory cytokine
743 bias in placenta and amniotic fluid. J Infect Dis. 2012;205(8):1305-10. Epub 20120301. doi:
744 10.1093/infdis/jis186. PubMed PMID: 22383678.
745 23. Gervasi MT, Romero R, Bracalente G, Chaiworapongsa T, Erez O, Dong Z, et al. Viral
746 invasion of the amniotic cavity (VIAC) in the midtrimester of pregnancy. J Matern Fetal Neonatal
747 Med. 2012;25(10):2002-13. Epub 20120530. doi: 10.3109/14767058.2012.683899. PubMed
748 PMID: 22524157; PubMed Central PMCID: PMCPMC3498469.
749 24. Bourgon N, Fitzgerald W, Aschard H, Magny JF, Guilleminot T, Stirnemann J, et al.
750 Cytokine Profiling of Amniotic Fluid from Congenital Cytomegalovirus Infection. Viruses.
751 2022;14(10). Epub 20220928. doi: 10.3390/v14102145. PubMed PMID: 36298700; PubMed
752 Central PMCID: PMCPMC9607316.
753 25. Weisblum Y, Panet A, Zakay-Rones Z, Vitenshtein A, Haimov-Kochman R, Goldman-
754 Wohl D, et al. Human cytomegalovirus induces a distinct innate immune response in the
755 maternal-fetal interface. Virology. 2015;485:289-96. Epub 20150828. doi:
756 10.1016/j.virol.2015.06.023. PubMed PMID: 26318261.
757 26. Weisblum Y, Oiknine-Djian E, Vorontsov OM, Haimov-Kochman R, Zakay-Rones Z, Meir
758 K, et al. Zika Virus Infects Early- and Midgestation Human Maternal Decidual Tissues, Inducing
759 Distinct Innate Tissue Responses in the Maternal-Fetal Interface. J Virol. 2017;91(4):e01905-16.
760 Epub 20170131. doi: 10.1128/JVI.01905-16. PubMed PMID: 27974560; PubMed Central
761 PMCID: PMCPMC5286880.

762 27. Yockey LJ, Jurado KA, Arora N, Millet A, Rakib T, Milano KM, et al. Type I interferons
763 instigate fetal demise after Zika virus infection. Sci Immunol. 2018;3(19). Epub 2018/01/07. doi:
764 10.1126/sciimmunol.aao1680. PubMed PMID: 29305462; PubMed Central PMCID:
765 PMCPMC6049088.
766 28. Rowe JH, Ertelt JM, Xin L, Way SS. Listeria monocytogenes cytoplasmic entry induces
767 fetal wastage by disrupting maternal Foxp3+ regulatory T cell-sustained fetal tolerance. PLoS
768 Pathog. 2012;8(8):e1002873. Epub 20120816. doi: 10.1371/journal.ppat.1002873. PubMed
769 PMID: 22916020; PubMed Central PMCID: PMCPMC3420962.
770 29. Schleiss MR. Nonprimate models of congenital cytomegalovirus (CMV) infection: gaining
771 insight into pathogenesis and prevention of disease in newborns. ILAR J. 2006;47(1):65-72.
772 Epub 2006/01/05. doi: 10.1093/ilar.47.1.65. PubMed PMID: 16391432.
773 30. Morrison JL, Botting KJ, Darby JRT, David AL, Dyson RM, Gatford KL, et al. Guinea pig
774 models for translation of the developmental origins of health and disease hypothesis into the
775 clinic. J Physiol. 2018;596(23):5535-69. Epub 20180530. doi: 10.1113/JP274948. PubMed
776 PMID: 29633280; PubMed Central PMCID: PMCPMC6265540.
777 31. Hartley JW, Rowe WP, Huebner RJ. Serial propagation of the guinea pig salivary gland
778 virus in tissue culture. Proc Soc Exp Biol Med. 1957;96(2):281-5. Epub 1957/11/01. doi:
779 10.3181/00379727-96-23455. PubMed PMID: 13485080.
780 32. Choi YC, Hsiung GD. Cytomegalovirus infection in guinea pigs. II. Transplacental and
781 horizontal transmission. J Infect Dis. 1978;138(2):197-202. Epub 1978/08/01. doi:
782 10.1093/infdis/138.2.197. PubMed PMID: 210239.
783 33. Griffith BP, McCormick SR, Fong CK, Lavallee JT, Lucia HL, Goff E. The placenta as a
784 site of cytomegalovirus infection in guinea pigs. J Virol. 1985;55(2):402-9. Epub 1985/08/01. doi:
785 10.1128/JVI.55.2.402-409.1985. PubMed PMID: 2991565; PubMed Central PMCID:
786 PMCPMC254947.

787 34. Auerbach MR, Yan D, Vij R, Hongo JA, Nakamura G, Vernes JM, et al. A neutralizing
788 anti-gH/gL monoclonal antibody is protective in the guinea pig model of congenital CMV
789 infection. PLoS Pathog. 2014;10(4):e1004060. Epub 20140410. doi:
790 10.1371/journal.ppat.1004060. PubMed PMID: 24722349; PubMed Central PMCID:
791 PMCPMC3983071.
792 35. Griffith BP, Lucia HL, Hsiung GD. Brain and visceral involvement during congenital
793 cytomegalovirus infection of guinea pigs. Pediatr Res. 1982;16(6):455-9. Epub 1982/06/01. doi:
794 10.1203/00006450-198206000-00010. PubMed PMID: 6285263.
795 36. Griffith BP, Hsiung GD. Cytomegalovirus infection in guinea pigs. IV. Maternal infection
796 at different stages of gestation. J Infect Dis. 1980;141(6):787-93. Epub 1980/06/01. doi:
797 10.1093/infdis/141.6.787. PubMed PMID: 6248603.
798 37. Harrison CJ, Britt WJ, Chapman NM, Mullican J, Tracy S. Reduced congenital
799 cytomegalovirus (CMV) infection after maternal immunization with a guinea pig CMV
800 glycoprotein before gestational primary CMV infection in the guinea pig model. J Infect Dis.
801 1995;172(5):1212-20. Epub 1995/11/01. doi: 10.1093/infdis/172.5.1212. PubMed PMID:
802 7594656.
803 38. Berkebile ZW, Putri DS, Abrahante JE, Seelig DM, Schleiss MR, Bierle CJ. The
804 Placental Response to Guinea Pig Cytomegalovirus Depends Upon the Timing of Maternal
805 Infection. Front Immunol. 2021;12:686415. Epub 20210615. doi: 10.3389/fimmu.2021.686415.
806 PubMed PMID: 34211475; PubMed Central PMCID: PMCPMC8239309.
807 39. Coleman S, Choi KY, Root M, McGregor A. A Homolog Pentameric Complex Dictates
808 Viral Epithelial Tropism, Pathogenicity and Congenital Infection Rate in Guinea Pig
809 Cytomegalovirus. PLoS Pathog. 2016;12(7):e1005755. Epub 20160707. doi:
810 10.1371/journal.ppat.1005755. PubMed PMID: 27387220; PubMed Central PMCID:
811 PMCPMC4936736.

812 40. Hashimoto K, Yamada S, Katano H, Fukuchi S, Sato Y, Kato M, et al. Effects of
813 immunization of pregnant guinea pigs with guinea pig cytomegalovirus glycoprotein B on viral
814 spread in the placenta. Vaccine. 2013;31(31):3199-205. Epub 20130515. doi:
815 10.1016/j.vaccine.2013.04.078. PubMed PMID: 23684839.
816 41. Stahl PL, Salmen F, Vickovic S, Lundmark A, Navarro JF, Magnusson J, et al.
817 Visualization and analysis of gene expression in tissue sections by spatial transcriptomics.
818 Science. 2016;353(6294):78-82. Epub 2016/07/02. doi: 10.1126/science.aaf2403. PubMed
819 PMID: 27365449.
820 42. Bierle CJ, Fernandez-Alarcon C, Hernandez-Alvarado N, Zabeli JC, Janus BC, Putri DS,
821 Schleiss MR. Assessing Zika virus replication and the development of Zika-specific antibodies
822 after a mid-gestation viral challenge in guinea pigs. PLoS One. 2017;12(11):e0187720. Epub
823 20171103. doi: 10.1371/journal.pone.0187720. PubMed PMID: 29099873; PubMed Central
824 PMCID: PMCPMC5669436.
825 43. Putri DS, Berkebile ZW, Mustafa HJ, Fernandez-Alarcon C, Abrahante JE, Schleiss MR,
826 Bierle CJ. Cytomegalovirus infection elicits a conserved chemokine response from human and
827 guinea pig amnion cells. Virology. 2020;548:93-100. Epub 20200617. doi:
828 10.1016/j.virol.2020.06.005. PubMed PMID: 32838950; PubMed Central PMCID:
829 PMCPMC7447834.
830 44. Depreux FF, Czech L, Whitlon DS. Sex Genotyping of Archival Fixed and
831 Immunolabeled Guinea Pig Cochleas. Sci Rep. 2018;8(1):5156. Epub 20180326. doi:
832 10.1038/s41598-018-23491-3. PubMed PMID: 29581456; PubMed Central PMCID:
833 PMCPMC5980087.
834 45. Alam SM, Konno T, Rumi MA, Dong Y, Weiner CP, Soares MJ. Prolactin family of the
835 guinea pig, Cavia porcellus. Endocrinology. 2010;151(8):3918-28. Epub 20100609. doi:
836 10.1210/en.2010-0239. PubMed PMID: 20534723; PubMed Central PMCID:
837 PMCPMC2940522.

838 46. Raudvere U, Kolberg L, Kuzmin I, Arak T, Adler P, Peterson H, Vilo J. g:Profiler: a web
839 server for functional enrichment analysis and conversions of gene lists (2019 update). Nucleic
840 Acids Res. 2019;47(W1):W191-W8. Epub 2019/05/09. doi: 10.1093/nar/gkz369. PubMed PMID:
841 31066453; PubMed Central PMCID: PMCPMC6602461.
842 47. Schleiss MR, Aronow BJ, Handwerger S. Cytomegalovirus infection of human
843 syncytiotrophoblast cells strongly interferes with expression of genes involved in placental
844 differentiation and tissue integrity. Pediatr Res. 2007;61(5 Pt 1):565-71. Epub 2007/04/07. doi:
845 10.1203/pdr.0b013e318045be6d. PubMed PMID: 17413859.
846 48. Alfi O, Cohen M, Bar-On S, Hashimshony T, Levitt L, Raz Y, et al. Decidual-tissue-
847 resident memory T cells protect against nonprimary human cytomegalovirus infection at the
848 maternal-fetal interface. Cell Rep. 2024;43(2):113698. Epub 20240123. doi:
849 10.1016/j.celrep.2024.113698. PubMed PMID: 38265934.
850 49. Lopez H, Benard M, Saint-Aubert E, Baron M, Martin H, Al Saati T, et al. Novel model of
851 placental tissue explants infected by cytomegalovirus reveals different permissiveness in early
852 and term placentae and inhibition of indoleamine 2,3-dioxygenase activity. Placenta.
853 2011;32(7):522-30. Epub 20110524. doi: 10.1016/j.placenta.2011.04.016. PubMed PMID:
854 21605903.
855 50. Hemmings DG, Kilani R, Nykiforuk C, Preiksaitis J, Guilbert LJ. Permissive
856 cytomegalovirus infection of primary villous term and first trimester trophoblasts. J Virol.
857 1998;72(6):4970-9. Epub 1998/05/30. doi: 10.1128/JVI.72.6.4970-4979.1998. PubMed PMID:
858 9573266; PubMed Central PMCID: PMCPMC110059.
859 51. Barrozo ER, Seferovic MD, Castro ECC, Major AM, Moorshead DN, Jochum MD, et al.
860 SARS-CoV-2 niches in human placenta revealed by spatial transcriptomics. Med.
861 2023;4(9):612-34 e4. Epub 20230708. doi: 10.1016/j.medj.2023.06.003. PubMed PMID:
862 37423216; PubMed Central PMCID: PMCPMC10527005.

863 52. Schafer H, Burger R. Tools for cellular immunology and vaccine research the in the
864 guinea pig: monoclonal antibodies to cell surface antigens and cell lines. Vaccine.
865 2012;30(40):5804-11. Epub 20120720. doi: 10.1016/j.vaccine.2012.07.012. PubMed PMID:
866 22819989.
867 53. Hilton HG, Rubinstein ND, Janki P, Ireland AT, Bernstein N, Fong NL, et al. Single-cell
868 transcriptomics of the naked mole-rat reveals unexpected features of mammalian immunity.
869 PLoS Biol. 2019;17(11):e3000528. Epub 20191121. doi: 10.1371/journal.pbio.3000528.
870 PubMed PMID: 31751331; PubMed Central PMCID: PMCPMC6894886.
871 54. Moses L, Pachter L. Museum of spatial transcriptomics. Nat Methods. 2022;19(5):534-
872 46. Epub 20220310. doi: 10.1038/s41592-022-01409-2. PubMed PMID: 35273392.
873 55. Arutyunyan A, Roberts K, Troule K, Wong FCK, Sheridan MA, Kats I, et al. Spatial
874 multiomics map of trophoblast development in early pregnancy. Nature. 2023;616(7955):143-
875 51. Epub 20230329. doi: 10.1038/s41586-023-05869-0. PubMed PMID: 36991123; PubMed
876 Central PMCID: PMCPMC10076224.
877 56. Vento-Tormo R, Efremova M, Botting RA, Turco MY, Vento-Tormo M, Meyer KB, et al.
878 Single-cell reconstruction of the early maternal-fetal interface in humans. Nature.
879 2018;563(7731):347-53. Epub 20181114. doi: 10.1038/s41586-018-0698-6. PubMed PMID:
880 30429548; PubMed Central PMCID: PMCPMC7612850.
881 57. Pique-Regi R, Romero R, Tarca AL, Sendler ED, Xu Y, Garcia-Flores V, et al. Single cell
882 transcriptional signatures of the human placenta in term and preterm parturition. Elife. 2019;8.
883 Epub 20191212. doi: 10.7554/eLife.52004. PubMed PMID: 31829938; PubMed Central PMCID:
884 PMCPMC6949028.
885 58. Pique-Regi R, Romero R, Tarca AL, Luca F, Xu Y, Alazizi A, et al. Does the human
886 placenta express the canonical cell entry mediators for SARS-CoV-2? Elife. 2020;9:e58716.
887 Epub 20200714. doi: 10.7554/eLife.58716. PubMed PMID: 32662421; PubMed Central PMCID:
888 PMCPMC7367681.

889 59. Marsh B, Blelloch R. Single nuclei RNA-seq of mouse placental labyrinth development.
890 Elife. 2020;9. Epub 20201103. doi: 10.7554/eLife.60266. PubMed PMID: 33141023; PubMed
891 Central PMCID: PMCPMC7669270.
892 60. Pereira L, Maidji E, McDonagh S, Genbacev O, Fisher S. Human cytomegalovirus
893 transmission from the uterus to the placenta correlates with the presence of pathogenic bacteria
894 and maternal immunity. J Virol. 2003;77(24):13301-14. doi: 10.1128/jvi.77.24.13301-
895 13314.2003. PubMed PMID: 14645586; PubMed Central PMCID: PMCPMC296088.
896 61. Gil-Sanchez A, Koletzko B, Larque E. Current understanding of placental fatty acid
897 transport. Curr Opin Clin Nutr Metab Care. 2012;15(3):265-72. Epub 2012/03/28. doi:
898 10.1097/MCO.0b013e3283523b6e. PubMed PMID: 22450774.
899 62. Herrera E. Lipid metabolism in pregnancy and its consequences in the fetus and
900 newborn. Endocrine. 2002;19(1):43-55. Epub 2003/02/14. doi: 10.1385/ENDO:19:1:43. PubMed
901 PMID: 12583601.
902 63. Ziaei S, Bonab KM, Kazemnejad A. Serum lipid levels at 28-32 weeks gestation and
903 hypertensive disorders. Hypertens Pregnancy. 2006;25(1):3-10. Epub 2006/04/15. doi:
904 10.1080/10641950500543756. PubMed PMID: 16613787.
905 64. Ray JG, Diamond P, Singh G, Bell CM. Brief overview of maternal triglycerides as a risk
906 factor for pre-eclampsia. BJOG. 2006;113(4):379-86. Epub 2006/03/24. doi: 10.1111/j.1471-
907 0528.2006.00889.x. PubMed PMID: 16553649.
908 65. Catov JM, Bodnar LM, Kip KE, Hubel C, Ness RB, Harger G, Roberts JM. Early
909 pregnancy lipid concentrations and spontaneous preterm birth. Am J Obstet Gynecol.
910 2007;197(6):610 e1-7. Epub 2007/12/07. doi: 10.1016/j.ajog.2007.04.024. PubMed PMID:
911 18060950.
912 66. Lange PT, Lagunoff M, Tarakanova VL. Chewing the Fat: The Conserved Ability of DNA
913 Viruses to Hijack Cellular Lipid Metabolism. Viruses. 2019;11(2). Epub 20190129. doi:
914 10.3390/v11020119. PubMed PMID: 30699959; PubMed Central PMCID: PMCPMC6409581.

915 67. Munger J, Bennett BD, Parikh A, Feng XJ, McArdle J, Rabitz HA, et al. Systems-level
916 metabolic flux profiling identifies fatty acid synthesis as a target for antiviral therapy. Nat
917 Biotechnol. 2008;26(10):1179-86. Epub 20080928. doi: 10.1038/nbt.1500. PubMed PMID:
918 18820684; PubMed Central PMCID: PMCPMC2825756.
919 68. Abrahamsen LH, Clay MJ, Lyle JM, Zink JM, Fredrikson LJ, DeSiervo AJ, Jerkofsky MA.
920 The effects of cytomegalovirus infection on polar lipids and neutral lipids in cultured human
921 cells. Intervirology. 1996;39(4):223-9. Epub 1996/01/01. doi: 10.1159/000150521. PubMed
922 PMID: 9078462.
923 69. Gudleski-O'Regan N, Greco TM, Cristea IM, Shenk T. Increased expression of LDL
924 receptor-related protein 1 during human cytomegalovirus infection reduces virion cholesterol
925 and infectivity. Cell Host Microbe. 2012;12(1):86-96. Epub 2012/07/24. doi:
926 10.1016/j.chom.2012.05.012. PubMed PMID: 22817990; PubMed Central PMCID:
927 PMCPMC3405916.
928 70. Low H, Mukhamedova N, Cui HL, McSharry BP, Avdic S, Hoang A, et al.
929 Cytomegalovirus Restructures Lipid Rafts via a US28/CDC42-Mediated Pathway, Enhancing
930 Cholesterol Efflux from Host Cells. Cell Rep. 2016;16(1):186-200. Epub 20160616. doi:
931 10.1016/j.celrep.2016.05.070. PubMed PMID: 27320924; PubMed Central PMCID:
932 PMCPMC5389417.
933 71. Chen Q, Gouilly J, Ferrat YJ, Espino A, Glaziou Q, Cartron G, et al. Metabolic
934 reprogramming by Zika virus provokes inflammation in human placenta. Nat Commun.
935 2020;11(1):2967. Epub 20200611. doi: 10.1038/s41467-020-16754-z. PubMed PMID:
936 32528049; PubMed Central PMCID: PMCPMC7290035.
937 72. Maxwell AJ, You Y, Aldo PB, Zhang Y, Ding J, Mor G. The role of the immune system
938 during pregnancy: General concepts. In: Mor G, editor. Reproductive Immunology: Academic
939 Press; 2021. p. 1-21.

940 73. Gomez-Lopez N, Romero R. The nature of the immune response in microbial-associated
941 and sterile intraamniotic inflammation. In: Mor G, editor. Reproductive Immunology: Academic
942 Press; 2021. p. 207-37.
943 74. Bao M, Hofsink N, Plosch T. LPS versus Poly I:C model: comparison of long-term effects
944 of bacterial and viral maternal immune activation on the offspring. Am J Physiol Regul Integr
945 Comp Physiol. 2022;322(2):R99-R111. Epub 20211207. doi: 10.1152/ajpregu.00087.2021.
946 PubMed PMID: 34874190; PubMed Central PMCID: PMCPMC8782664.
947 75. Miner JJ, Cao B, Govero J, Smith AM, Fernandez E, Cabrera OH, et al. Zika Virus
948 Infection during Pregnancy in Mice Causes Placental Damage and Fetal Demise. Cell.
949 2016;165(5):1081-91. Epub 20160511. doi: 10.1016/j.cell.2016.05.008. PubMed PMID:
950 27180225; PubMed Central PMCID: PMCPMC4874881.
951 76. Buchrieser J, Degrelle SA, Couderc T, Nevers Q, Disson O, Manet C, et al. IFITM
952 proteins inhibit placental syncytiotrophoblast formation and promote fetal demise. Science.
953 2019;365(6449):176-80. Epub 2019/07/13. doi: 10.1126/science.aaw7733. PubMed PMID:
954 31296770.
955 77. Rice G, Patrick T, Parmar R, Taylor CF, Aeby A, Aicardi J, et al. Clinical and molecular
956 phenotype of Aicardi-Goutieres syndrome. Am J Hum Genet. 2007;81(4):713-25. Epub
957 20070904. doi: 10.1086/521373. PubMed PMID: 17846997; PubMed Central PMCID:
958 PMCPMC2227922.
959 78. Kim CJ, Romero R, Kusanovic JP, Yoo W, Dong Z, Topping V, et al. The frequency,
960 clinical significance, and pathological features of chronic chorioamnionitis: a lesion associated
961 with spontaneous preterm birth. Mod Pathol. 2010;23(7):1000-11. Epub 20100326. doi:
962 10.1038/modpathol.2010.73. PubMed PMID: 20348884; PubMed Central PMCID:
963 PMCPMC3096929.
964 79. Romero R, Chaemsaithong P, Chaiyasit N, Docheva N, Dong Z, Kim CJ, et al. CXCL10
965 and IL-6: Markers of two different forms of intra-amniotic inflammation in preterm labor. Am J

966 Reprod Immunol. 2017;78(1):e12685. Epub 20170519. doi: 10.1111/aji.12685. PubMed PMID:
967 28544362; PubMed Central PMCID: PMCPMC5488235.
968 80. Maymon E, Romero R, Bhatti G, Chaemsaithong P, Gomez-Lopez N, Panaitescu B, et
969 al. Chronic inflammatory lesions of the placenta are associated with an up-regulation of amniotic
970 fluid CXCR3: A marker of allograft rejection. J Perinat Med. 2018;46(2):123-37. Epub
971 2017/08/23. doi: 10.1515/jpm-2017-0042. PubMed PMID: 28829757; PubMed Central PMCID:
972 PMCPMC5797487.
973 81. Hirsch AJ, Roberts VHJ, Grigsby PL, Haese N, Schabel MC, Wang X, et al. Zika virus
974 infection in pregnant rhesus macaques causes placental dysfunction and immunopathology. Nat
975 Commun. 2018;9(1):263. Epub 20180117. doi: 10.1038/s41467-017-02499-9. PubMed PMID:
976 29343712; PubMed Central PMCID: PMCPMC5772047.
977 82. Manuel T, Mostrom M, Crooks CM, Davalos A, Barfield R, Scheef E, et al. A nonhuman
978 primate model mirrors human congenital cytomegalovirus infection and reveals a spectrum of
979 vertical transmission outcomes. bioRxiv. 2025:2025.01.16.633406. Epub 20250121. doi:
980 10.1101/2025.01.16.633406. PubMed PMID: 40492197; PubMed Central PMCID:
981 PMCPMC12148051.
982 83. Adkins RM, Walton AH, Honeycutt RL. Higher-level systematics of rodents and
983 divergence time estimates based on two congruent nuclear genes. Mol Phylogenet Evol.
984 2003;26(3):409-20. Epub 2003/03/20. doi: 10.1016/s1055-7903(02)00304-4. PubMed PMID:
985 12644400.
986 84. Roberts RM, Green JA, Schulz LC. The evolution of the placenta. Reproduction.
987 2016;152(5):R179-89. Epub 20160802. doi: 10.1530/REP-16-0325. PubMed PMID: 27486265;
988 PubMed Central PMCID: PMCPMC5033709.
989 85. Crumpler MM, Choi KY, McVoy MA, Schleiss MR. A live guinea pig cytomegalovirus
990 vaccine deleted of three putative immune evasion genes is highly attenuated but remains
991 immunogenic in a vaccine/challenge model of congenital cytomegalovirus infection. Vaccine.

992 2009;27(31):4209-18. Epub 20090503. doi: 10.1016/j.vaccine.2009.04.036. PubMed PMID:
993 19389443; PubMed Central PMCID: PMCPMC3539795.
994 86. Leviton MP, Lacayo JC, Choi KY, Hernandez-Alvarado N, Wey A, Schleiss MR. An
995 attenuated cytomegalovirus vaccine with a deletion of a viral chemokine gene is protective
996 against congenital CMV transmission in a guinea pig model. Clin Dev Immunol.
997 2013;2013:906948. Epub 20130820. doi: 10.1155/2013/906948. PubMed PMID: 24000289;
998 PubMed Central PMCID: PMCPMC3755440.
999 87. Pouliot N, Maghni K, Blanchette F, Cironi L, Sirois P, Stankova J, Rola-Pleszczynski M.
1000 Natural killer and lectin-dependent cytotoxic activities of Kurloff cells: target cell selectivity,
1001 conjugate formation, and Ca++ dependency. Inflammation. 1996;20(6):647-71. Epub
1002 1996/12/01. doi: 10.1007/BF01488802. PubMed PMID: 8979153.
1003 88. Marshall AH, Swettenham KV, Vernon-Roberts B, Revell PA. Studies on the function of
1004 the Kurloff cell. Int Arch Allergy Appl Immunol. 1971;40(1):137-52. doi: 10.1159/000230401.
1005 PubMed PMID: 4100635.
1006 89. Revell PA, Vernon-Roberts B, Gray A. The distribution and ultrastructure of the Kurloff
1007 cell in the guinea-pig. J Anat. 1971;109(Pt 2):187-99. Epub 1971/07/01. PubMed PMID:
1008 5558229; PubMed Central PMCID: PMCPMC1270999.
1009 90. Yang D, Tamburro K, Dittmer D, Cui X, McVoy MA, Hernandez-Alvarado N, Schleiss
1010 MR. Complete genome sequence of pathogenic Guinea pig cytomegalovirus from salivary gland
1011 homogenates of infected animals. Genome Announc. 2013;1(2):e0005413. Epub 20130314.
1012 doi: 10.1128/genomeA.00054-13. PubMed PMID: 23516193; PubMed Central PMCID:
1013 PMCPMC3622957.
1014 91. Martinez-Pacheco M, Tenorio M, Almonte L, Fajardo V, Godinez A, Fernandez D, et al.
1015 Expression Evolution of Ancestral XY Gametologs across All Major Groups of Placental
1016 Mammals. Genome Biol Evol. 2020;12(11):2015-28. Epub 2020/08/14. doi:
1017 10.1093/gbe/evaa173. PubMed PMID: 32790864; PubMed Central PMCID: PMCPMC7674692.

1018 92. Hafemeister C, Satija R. Normalization and variance stabilization of single-cell RNA-seq
1019 data using regularized negative binomial regression. Genome Biol. 2019;20(1):296. Epub
1020 20191223. doi: 10.1186/s13059-019-1874-1. PubMed PMID: 31870423; PubMed Central
1021 PMCID: PMCPMC6927181.
1022 93. Stuart T, Butler A, Hoffman P, Hafemeister C, Papalexi E, Mauck WM, 3rd, et al.
1023 Comprehensive Integration of Single-Cell Data. Cell. 2019;177(7):1888-902 e21. Epub
1024 20190606. doi: 10.1016/j.cell.2019.05.031. PubMed PMID: 31178118; PubMed Central PMCID:
1025 PMCPMC6687398.

1026

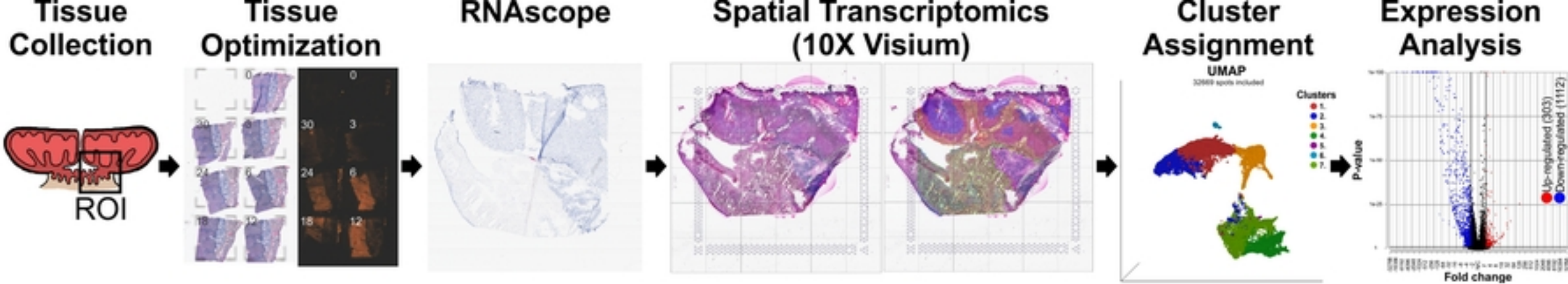
Tissue Collection
ROI
Tissue Optimization
RNAscope
Spatial Transcriptomics (10X Visium)
Cluster Assignment
UMAP
Clusters
Expression Analysis
P-value
Fold change
Up-regulated (303)
Down-regulated (1112)

Figure 1

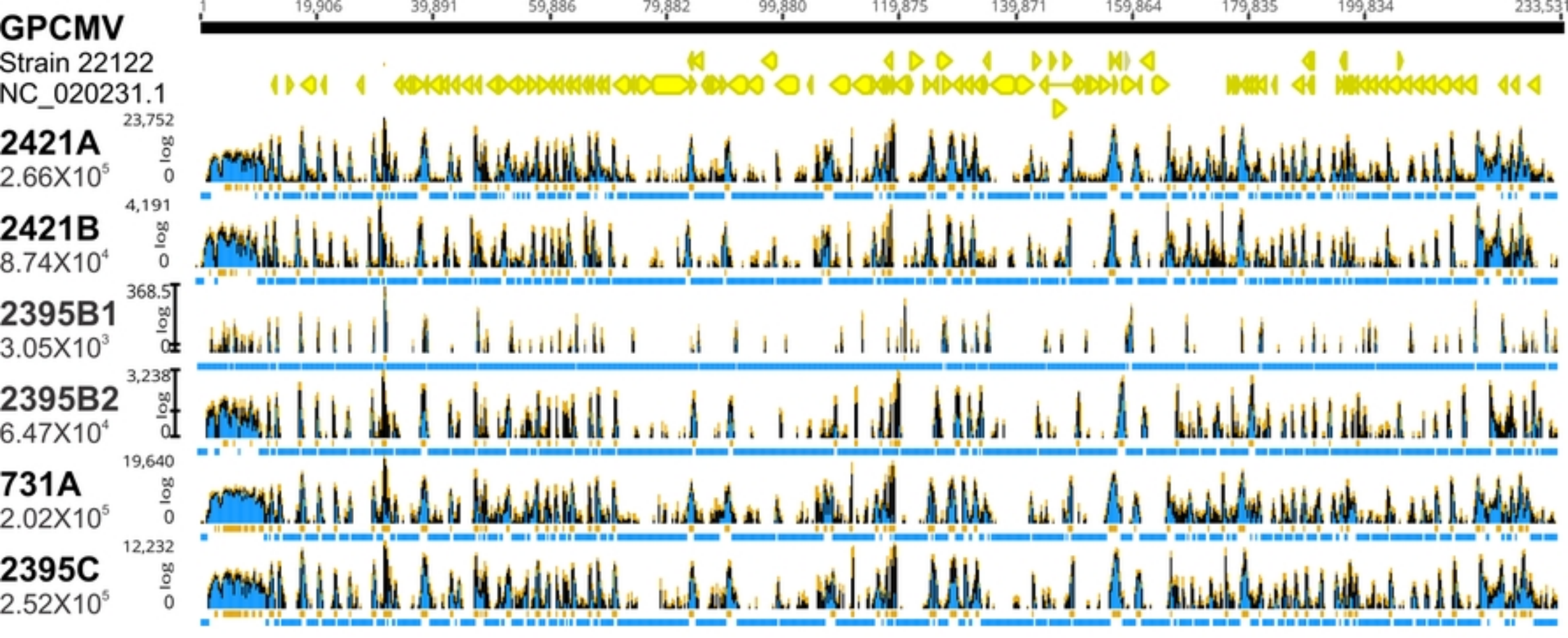
GPCMV
Strain 22122
NC_020231.1
1
19,906
39,891
59,886
79,882
99,880
119,875
139,871
159,864
179,835
199,834
233,53
2421A
2.66X10^5
23,752
log
0
2421B
8.74X10^4
4,191
log
0
2395B1
3.05X10^3
368.5
log
0
2395B2
6.47X10^4
3,238
log
0
731A
2.02X10^5
19,640
log
0
2395C
2.52X10^5
12,232
log
0

Figure 2

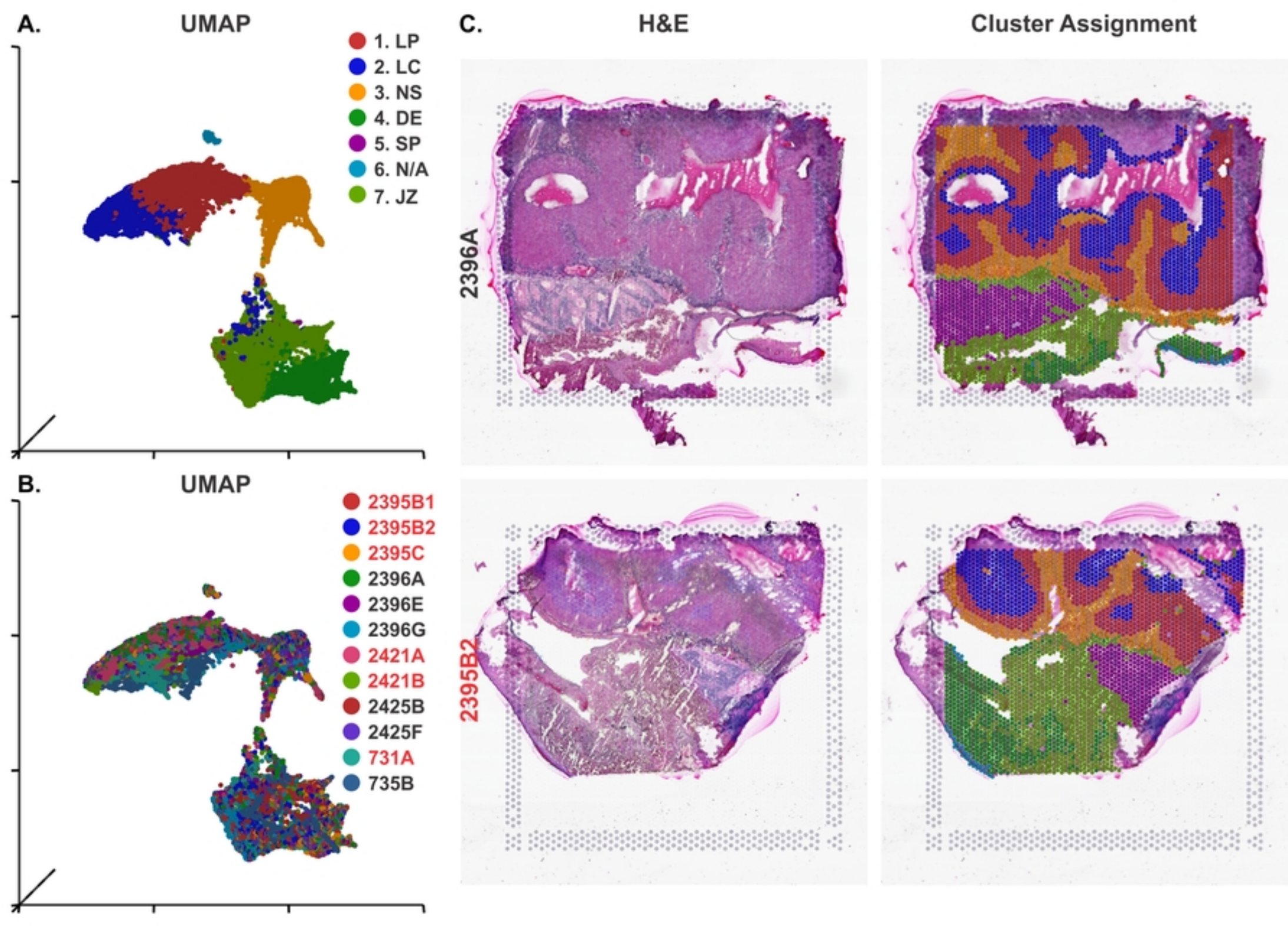
A.
UMAP
1. LP
2. LC
3. NS
4. DE
5. SP
6. N/A
7. JZ
B.
UMAP
2395B1
2395B2
2395C
2396A
2396E
2396G
2421A
2421B
2425B
2425F
731A
735B
C.
H&E
Cluster Assignment
2396A
2395B2

Figure 3

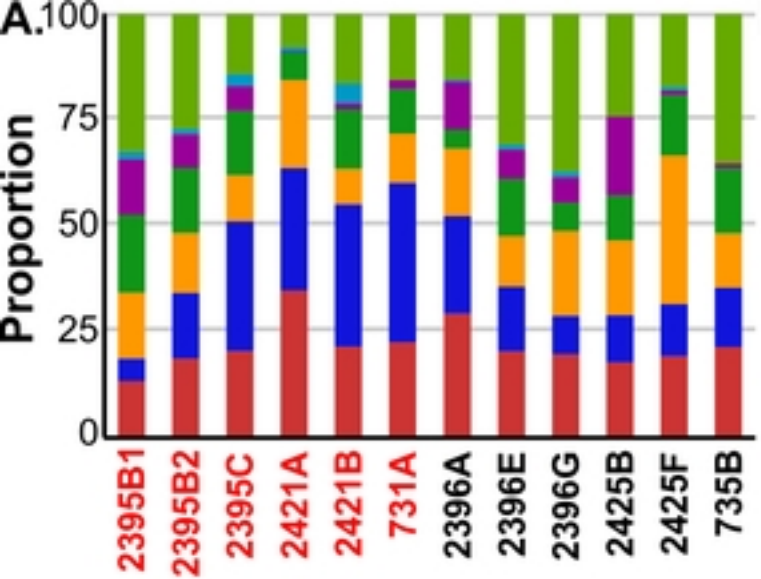

B.

Cluster	# Spots (CMV/Mock)	Up-Regulated	Down-Regulated
1. LP	3508 / 3685	42	87
2. LC	3868 / 2442	43	61
3. NS	2247 / 3152	48	82
4. DE	2121 / 1706	303	1112
5. SP	859 / 1168	100	134
6. N/A	278 / 110	ND	ND
7. JZ	3054 / 4420	281	585

Figure 4

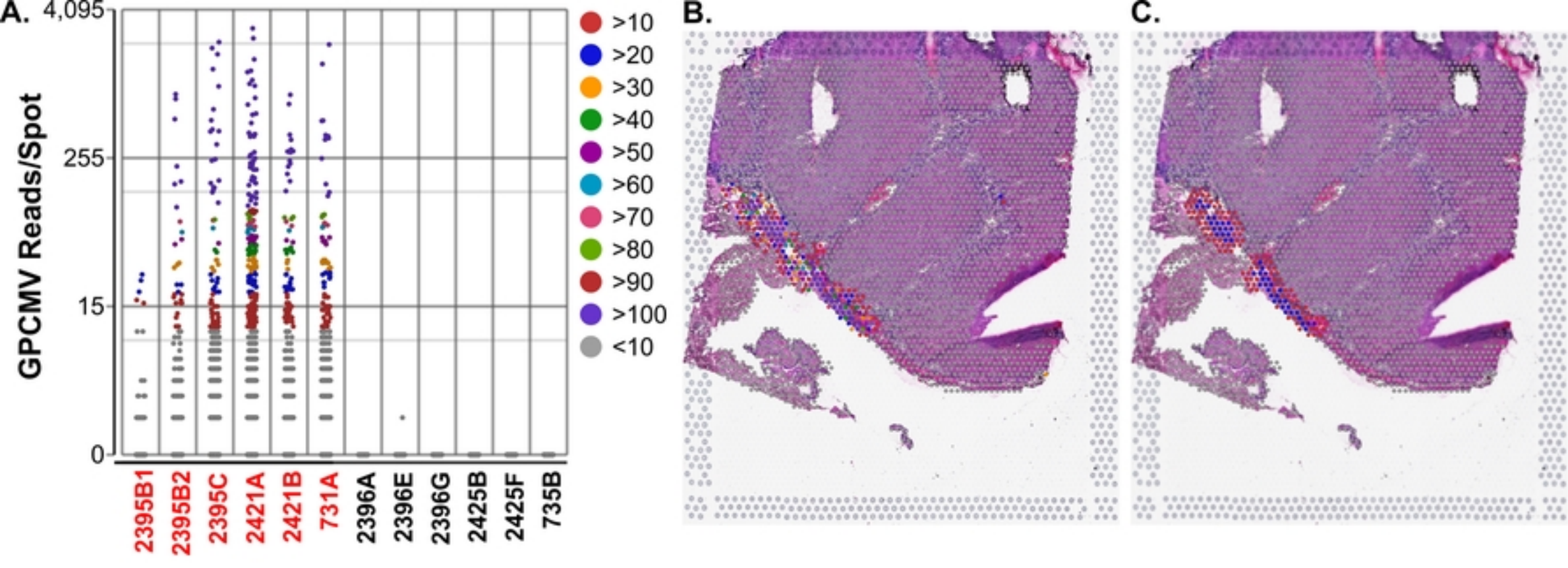
A.
4,095
255
15
0
GPCMV Reads/Spot
2395B1
2395B2
2395C
2421A
2421B
731A
2396A
2396E
2396G
2425B
2425F
735B
>10
>20
>30
>40
>50
>60
>70
>80
>90
>100
<10
B.
C.

Figure 5

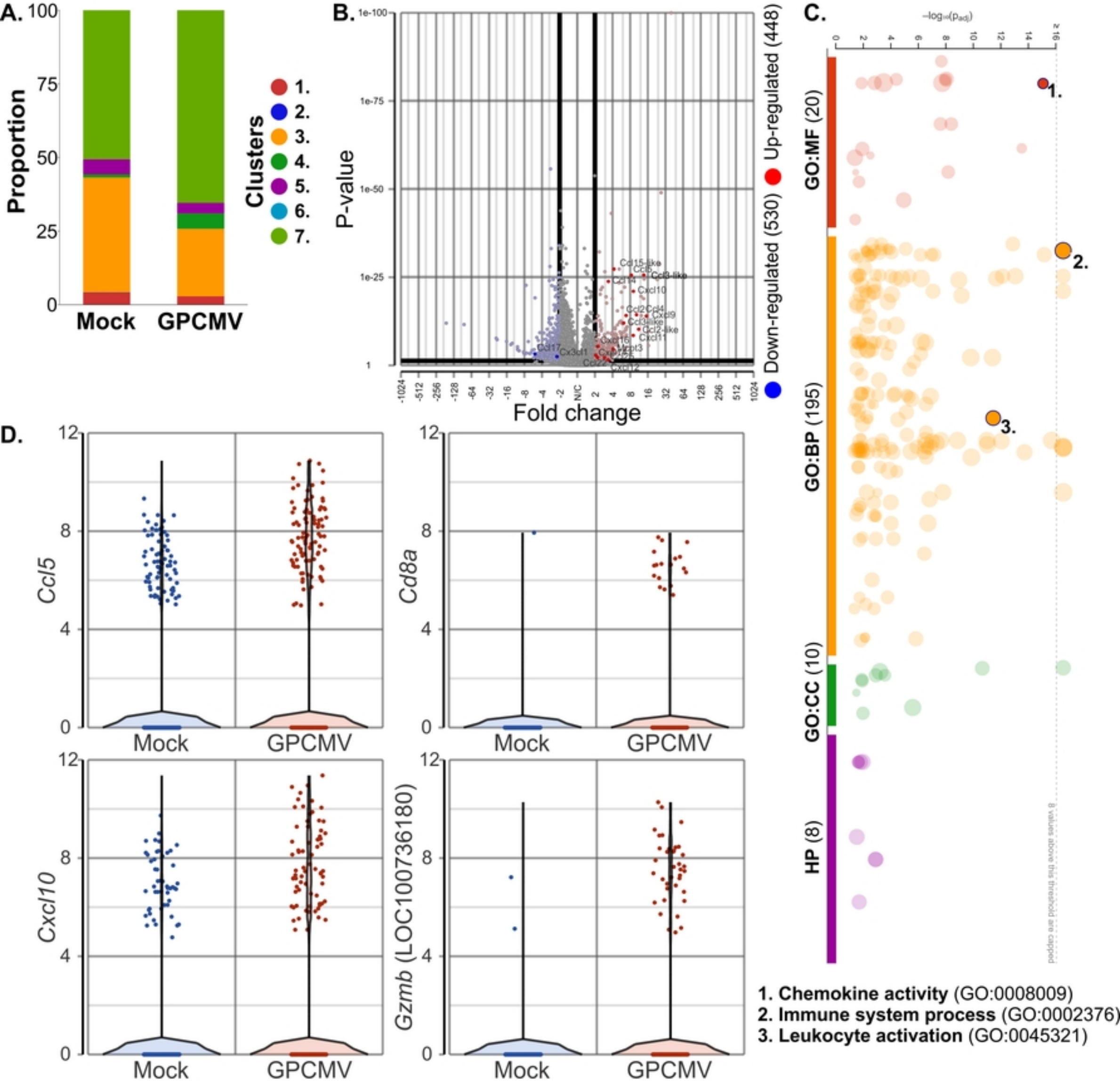
A.
Proportion
Mock
GPCMV
Clusters
1.
2.
3.
4.
5.
6.
7.
B.
P-value
Fold change
Up-regulated (448)
Down-regulated (530)
C.
GO:MF (20)
GO:BP (195)
GO:CC (10)
HP (8)
1. Chemokine activity (GO:0008009)
2. Immune system process (GO:0002376)
3. Leukocyte activation (GO:0045321)
D.
Ccl5
Cd8a
Cxcl10
Gzmb (LOC100736180)
Mock
GPCMV

Figure 6